Journal of Hydrology 603 (2021) 127162

Contents lists available at ScienceDirect

Journal of Hydrology

journal homepage: www.elsevier.com/locate/jhydrol

Research papers

A CONUS-scale study of wildfire and evapotranspiration: Spatial and temporal response and controlling factors

Natalie M. Collar [a,*], Samuel Saxe [b,a], Ashley J. Rust [a], Terri S. Hogue [a]

[a] Colorado School of Mines, Department of Civil and Environmental Engineering, 1500 Illinois St., Golden, CO 90336, USA
[b] US Geological Survey, Analysis and Prediction Branch, Lakewood, CO 80225, USA

ARTICLE INFO

This manuscript was handled by Sally Elizabeth Thompson, Editor-in-Chief, with the assistance of Xue Feng, Associate Editor

Keywords:
K-means clustering
Remote sensing
SSEBop
Post-fire
Machine learning
Disturbance hydrology

ABSTRACT

Evapotranspiration (ET) accounts for a substantial portion of regional water budgets in much of the southeast and fire-prone western United States (US). Even small changes in ET rates can translate to meaningful shifts in runoff patterns and makes forecasting the direction and magnitude of wildfire-induced ET alteration of critical importance. We use 1 km ET estimates from the operational Simplified Surface Energy Balance (SSEBop) product for the conterminous US (CONUS) to evaluate post-fire ET and evaporation ratio (ET/P) shifts in the first five post-fire years in approximately 5500 unique fires. Pixels with similar ET/P responses to fire are grouped through k-means clustering and the resultant cluster distribution is explored over space and time. The largest changes in post-fire ET/P are observed in the southwestern CONUS where first-year ratios are reduced by 50 to 90% and pre-fire ratios are rarely recovered by post-fire year five. Regional and intra-fire ET/P response variability is also highest in the western CONUS where climatic, topographic, and ecologic gradients are steep. Post-fire ET/P modifications are small to negligible in the east-southeast CONUS, and 18% of all pixels analyzed exhibit small to moderate increases in post-fire year one ET/P. A comparison of burned and unburned pixel pairs confirms the role of fire in the shifts but also indicates a high degree of background variability in the ET and precipitation data. Although the biggest percent ET/P reductions occur in shrub/scrub landscapes in much of the west, the biggest magnitude ET changes often occur in evergreen forests. Higher burn severities are consistently correlated with greater post-fire ET/P reductions, while relationships between post-fire ET/P shifts and numerous other landscape attributes (e.g., pre-fire vegetation type) vary in both direction and magnitude in different parts of the CONUS. Further work can be conducted to refine controlling relationships within more homogeneous sub-regions.

1. Introduction

Fire impacts the response of a landscape to precipitation by altering processes that partition water in the environment (DeBano et al., 1998). Evapotranspiration (ET), the component of the water budget most sensitive to vegetation changes (DeBano et al., 1998), can shift in direction and magnitude following fire-induced modifications to surface cover, the physical and chemical composition of the subsurface, and the local microclimate (Häusler et al., 2018; Sanford and Selnick, 2013; Shakesby and Doerr, 2006). Because ET can comprise a large fraction of local and regional water budgets, downstream water supplies can be impacted when that flux is disrupted (Blount et al., 2020; Kettridge et al., 2017; Martin, 2016; Moritz et al., 2014). The conterminous United States (CONUS) is particularly vulnerable to water supply disruptions from

Abbreviations: ET_a, actual evapotranspiration; AWC, available water capacity; BAER, Burned Area Emergency Response; CONUS, conterminous United States; ET/P, evaporation ratio; gNATSGO, Gridded National Soil Survey Geographic Database; IQR, interquartile range; LST, land surface temperature; ML, machine learning; METRIC, Mapping EvapoTranspiration at high Resolution with Internalized Calibration model; MTBS, Monitoring Trends in Burn Severity; MLR, multiple linear regression; NCAR, National Center for Atmospheric Research; NLCD, National Land Cover Database; NBR, normalized burn ratio; SSEBop, operational Simplified Surface Energy Balance Model; PDI, Palmer Drought Severity Index; PRISM, Parameter-elevation Regressions on Independent Slopes Model; ET_o, reference evapotranspiration; R80P, Ratio of 80% Pre-disturbance recovery metric; RMSE, root mean square error; RRI, Relative Recovery Indicator recovery metric; SNODAS, SNOw Data Assimilation model; SEB, surface energy balance; SEBAL, Surface Energy Balance Algorithm for Land model; HSD, Tukey's honestly significant difference; UCAR, University Corporation for Atmospheric Research; EROS, USGS Earth Resources Observing and Science center; YrYr, Year-on-Year Average recovery metric.

* Corresponding author.
E-mail addresses: ncollar@wrightwater.com (N.M. Collar), ssaxe@usgs.gov (S. Saxe), arust@mines.edu (A.J. Rust), thogue@mines.edu (T.S. Hogue).

https://doi.org/10.1016/j.jhydrol.2021.127162
Received 26 March 2021; Received in revised form 22 October 2021; Accepted 4 November 2021
Available online 10 November 2021

forest fires because forested areas supply approximately one-half of its surface freshwater supply (Hallema et al., 2018, 2017).

Prior work has confirmed the role of ET in post-disturbance water budget modification. Goeking and Tarboton (2020) reviewed studies on the effects of drought, beetle kill, and fire on water yield in western US forests and attribute the bulk of observed changes to ET shifts (Goeking and Tarboton, 2020). However, the vulnerability of a particular system or resource to fire-induced ET shifts depends on the context of the fire. If ET is reduced within a source water collection area, downstream water supply and quality may be compromised if surface runoff exacerbates erosion and increases reservoir sedimentation (Silins et al., 2009; Smith et al., 2011). Fires outside source water areas may degrade fragile terrestrial (Agee, 1994) or aquatic resources (Bixby et al., 2015) that provide ecosystem services. Variables such as the distance of the burn from the drainage outlet, size of the burned area relative to total drainage area, and post-fire climate, may also impact how vulnerable a system or resource is to fire-induced hydromodification (Brunkal and Santi, 2017; Minnich, 2001). ET shifts may be temporary (Blount et al., 2020), or conversion of forest to grassy or shrubby covers may permanently alter local and watershed-scale hydrology (Hankins, n.d.; Jones et al., 2020; Rodman et al., 2020).

Due to its high topographic, climatologic, and ecologic diversity, the range of abiotic and biotic factors that control water partitioning in the CONUS is wide (DeBano et al., 1998; Ma et al., 2020; Sellers, 1965). The effects of fire on ET and other hydrologic fluxes vary accordingly. Goeking and Tarboton (2020) cite instances where low flows, peak flows, and snow water equivalent (SWE) increased, decreased, or exhibited no change following disturbance. Mechanistically, fire can cause a net reduction in ET by removing vegetation or decreasing the amount of water available for transpiration or direct evaporation and sublimation losses (DeBano et al., 1998). This can lead to an increase in the fraction of precipitation that becomes surface runoff routed to reservoirs or made available for aquifer recharge (Blount et al., 2020; Boisramé et al., 2019; Hallema et al., 2018; Kinoshita and Hogue, 2015; Sanford and Selnick, 2013; Saxe et al., 2018). Pertinent on the global scale, post-fire ET reduction can disrupt global carbon cycling and, with increases in the frequency and severity of wildfires (Parks and Abatzoglou, 2020; Westerling, 2016), contribute to climate change by causing localized surface heating via latent heat flux reduction (Atchley et al., 2018; Bond-Lamberty et al., 2009; Grau Andres, 2017). Conversely, ET can increase where non-stand-replacing fires trigger rapid post-disturbance vegetation growth (Goeking and Tarboton, 2020; Nolan et al., 2015, 2014), where evaporative demand is high (e.g., on south-facing slopes or where vegetation structure and composition changes increase surface insolation (Goeking and Tarboton, 2020; Häusler et al., 2018)), or where canopy loss promotes snow accumulation and subsequent sublimation (Jin et al., 2012; Sexstone et al., 2018).

Several studies evaluate the effect of fire on ET at the sub-basin to regional scale. Ma et al. (2020) modeled ET reductions in the Sierra Nevada for up to 15 years following low to high severity burns. They attribute variations in the magnitude of reductions to differences in local hydro-climate, topography, pre-fire vegetation density, and severity of the disturbance (Ma et al., 2020). Poon and Kinoshita (2018) observed decreased ET and smaller evaporation ratios (the ratio of ET depth to precipitation depth for a unit area) across soil burn severities following post-fire conversion of coniferous forest to grassland in New Mexico. In Canadian boreal forest, although transpiration increased where fire converted mature conifer stands to young deciduous forest, Bond-Lamberty et al. (2009) observed a net decrease in ET at the regional scale due to the effects of fire on mean stand age, forest species, and energy balance (Bond-Lamberty et al., 2009). Häusler et al. (2018) and Nolan et al. (2014) studied Portuguese and Australian eucalyptus stands and observed increases in ET in low to moderate burn severity areas but reductions in high burn severity areas due to decreased latent heat flux from the canopy (Häusler et al., 2018; Nolan et al., 2014). These findings align with observations from others that post-fire ET shifts are often accompanied by fire-induced alterations to the variables that control surface energy partitioning, such as the reflective properties of a body (emissivity and albedo) or the amount of shortwave radiation delivered to objects and the ground surface (Dragosics et al., 2016; Häusler et al., 2018; Jin et al., 2012; Sexstone et al., 2018).

A portion of the post-fire ET response variability recorded in the CONUS may be explained by varying fire behavior and ignition sources. When fire size is plotted for every fire included in the Monitoring Trends in Burn Severity (MTBS) dataset for the CONUS (1984 through 2019), the median area increases nearly monotonically with more westerly longitudes (SM Figure A in Supplementary Materials). However, fire occurrence is relatively high in portions of both the western and eastern US. For example, of the fires included in the current study (all MTBS-mapped fires from 2006 to 2014 in the CONUS), 786 are located in Florida, 502 in Texas, 399 in California, 296 in Kansas, and 244 in Arizona (SM Table A). These summaries corroborate previous research (Hawbaker et al., 2013). Hawbaker et al. (2013) show that conducive fire weather conditions, forest densification, and abundant opportunities for human-caused ignitions due to extensive urban and suburban development, were the primary drivers of the southwestern US's large fire sizes.

As more work shows that common disturbances can alter the components of water and energy balances that control ET rates (including mountain bark beetle kill (Livneh et al., 2015) and climatic forcing (Fowler et al., 2018), in addition to fire), the importance of accounting for such perturbances in hydrologic modeling is becoming clearer. Over the last two decades, remotely sensed data have helped hydrologists study disturbance events by facilitating estimations of hydrologic fluxes at varying spatial and temporal extents. What were once prohibitive obstacles for disturbance-change monitoring studies, such as capturing the pre-disturbance condition, or observing remote locations, are now overcome with primary and reanalysis products that require limited to no post-processing. Regional-scale studies can be conducted from the desktop. The current study and many of the aforementioned (Blount et al., 2020; Poon and Kinoshita, 2018; Sexstone et al., 2018) utilize the United States Geological Survey's (USGS) operational 1 km^2 Simplified Surface Energy Balance (SSEBop) product. Others use satellite-retrieved reflectance data as inputs to independent ET calculations (Häusler et al., 2018) or large-scale modeling simulations (Bond-Lamberty et al., 2009). Goulden and Bales (2014) and Ma et al. (2020) developed statistical relationships between ground-based measurements of ET and satellite imagery-derived metrics (e.g., normalized difference vegetation index [NDVI]) to estimate ET in uninstrumented locations.

Despite the substantial effort spent quantifying fire's effect on basin to regional-scale ET, no studies identify super-regional-scale trends or evaluate the full range of conditions present in the CONUS. The current work aims to fill that gap by characterizing spatial and temporal post-fire ET response at the CONUS scale and numerous finer spatial extents. Our primary research questions include: **(i) How have historical wildfires modified the direction and magnitude of ET across the CONUS? (ii) Can we identify spatial or temporal trends that can help land managers plan for potential future post-fire water budget modifications?** And, **(iii) what controls the response?** These inquiries are relevant to natural resource managers in fire-prone areas who need to understand the potential hydrologic response of their landscape to wildfire. Identifying drivers of post-fire ET response can also inform process-based and statistical hydrologic modeling efforts.

2. Material and methods

We investigate the response of ET to fire using metrics calculated with per-pixel estimates of daily actual ET (ET_a) from the 1 km^2 SSEBop product and Parameter-elevation Regressions on Independent Slopes Model (PRISM) precipitation estimates (Oregon State University, Northwest Alliance for Computational Science and Engineering, 2019). Pixel-level differences of pre and post-fire ET_a and the ratio of ET_a to

precipitation ("ET/P," "evaporation ratio") are quantified for the first five post-fire years; previous studies have also used the evaporation ratio to normalize for climate variability (Blount et al., 2020; Poon and Kinoshita, 2018; Reitz et al., 2017). Machine learning (ML) methods are used to group pixels with similar magnitudes and directions of post-fire ET/P response. At every SSEBop pixel, pyrologic, topographic, and climatic data are resampled at the 1 km resolution and relationships between ET/P response and independent variables are evaluated.

2.1. Geospatial data collection and processing

2.1.1. Identification of ET_a data from burned areas

The MTBS fire data layer is used to identify burned areas in the CONUS from 2000 to 2015 (Eidenshink et al., 2007). MTBS maps the extent and burn severity of fires using Normalized Burn Ratio (NBR) and differenced Normalized Burn Ratio (dNBR) data generated from 30 m Landsat scenes. In this study, 1 km monthly SSEBop ET_a data are extracted from pixels that intersect burned 30 m MTBS pixels. Pixels are filtered to remove areas where more than one fire event occurred from 1999 to 2015 and pixels that are less than 75% burned (according to their intersection with MTBS fire perimeters). Fires that occurred before 2005 are removed so that only burned areas with five years of pre-fire ET_a data are retained. 140,509 1 km SSEBop pixels from 5390 individual fires remain for analysis (see pixel distribution in Fig. 1).

2.1.2. SSEBop

The USGS's operational 1 km monthly SSEBop ET_a product (Senay et al., 2013) is based on the Simplified Surface Energy Balance (SSEB) approach (Senay et al., 2007, 2011). Similar to the Surface Energy Balance Algorithm for Land (SEBAL) (Bastiaanssen et al., 1998) and Mapping EvapoTranspiration at high Resolution with Internalized Calibration (METRIC) (Allen et al., 2007) models, SSEBop utilizes hot (T_h) and cold (T_c) reference values to predefine temperature difference (dT) (boundary conditions) at each pixel under the assumption that dT is constant at a given location on the same day each year (Senay et al., 2007). Assumptions are made to allow for quantification of sensible heat flux and total net radiation, and each day's land surface temperature (LST) is compared to the hot pixel condition and dT to generate a monthly ET fraction. ET_a is calculated by multiplying the ET fraction with reference ET values (ET_o) from the USGS Earth Resources Observing and Science center (EROS) (Savoca et al., 2013; Senay et al., 2013, 2008).

The 1 km SSEBop product has been evaluated in numerous studies. SSEBop ET_a agreement with eddy covariance Ameriflux tower estimations located throughout the CONUS in varying climatic conditions and land cover classes was high (Chen et al., 2016; Savoca et al., 2013; Senay et al., 2013). Velpuri et al. (2013) report good agreement between 1 km Moderate Resolution Imaging Spectroradiometer (MODIS) global ET_a (MOD16), SSEBop ET_a, eddy covariance, and water balance data across the CONUS (Velpuri et al., 2013). Senkondo et al. (2019) report statistically comparable SSEBop, SEBAL, and Simplified Surface Balance Index (S-SEBI) ET_a estimates across different spatial scales and land cover classes in sub-tropical Tanzania (Senkondo et al., 2019). SSEBop's algorithm is also being applied with 30 m and 100 m Landsat LSTs (Dias Lopes et al., 2019; Senay et al., 2016, 2014; Sharma and Tare, 2018; Singh and Senay, 2015), although only a provisional product that is

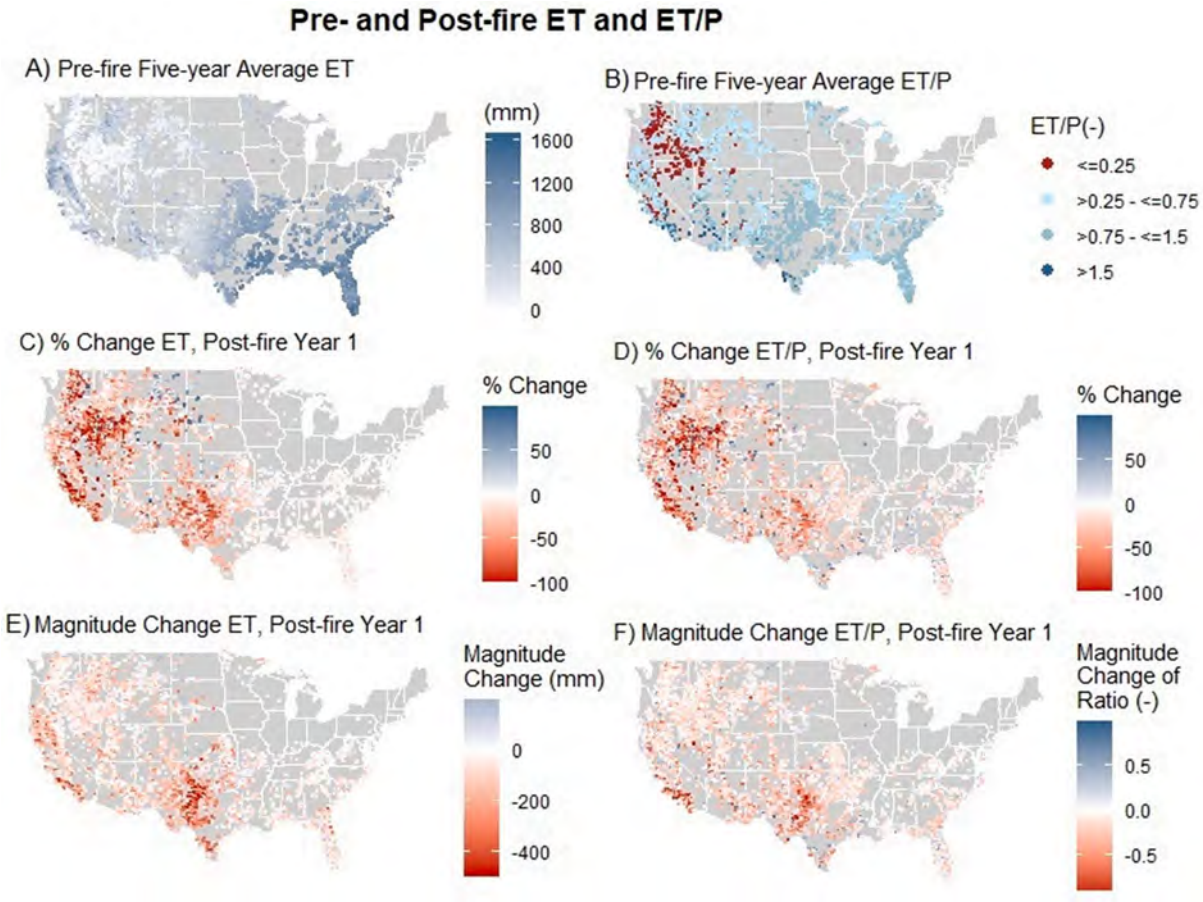

Fig. 1. Pre and initial post-fire ET and ET/P response for all pixels included in the study. (A) Pre-fire five-year average ET (ET_a); (B) pre-fire five-year average annual evaporation ratio (ET/P); (C) percent change in ET in post-fire year one; (D) percent change in ET/P in post-fire year; (E) magnitude change in ET in post-fire year one; (F) magnitude change in ET/P in post-fire year one.

subject to revision is currently available (USGS EROS Customer Services, n.d.).

2.1.3. Independent variables

Independent variables (landscape attributes) are extracted at each SSEBop pixel including burn severity, climatological descriptors, pre-fire vegetation type, topographical and positional descriptors, and soils and geology data. For each SSEBop pixel, extracted data are retained and stored as columns in a data frame (one row per pixel). Dependent and independent variable descriptions, data sources, processing requirements, units, and summary calculations are provided in Table 1. Except for aspect, data at spatial resolutions larger or smaller than the 1 km SSEBop pixels are disaggregated or upscaled by area-weighted averaging using the *raster* package in the R programming environment (Hijmans et al., 2021).

Details of each fire event (e.g., incident type (wildfire or prescribed fire), ignition date) and burn severity data are obtained from 30 m MTBS rasters (Eidenshink et al., 2007). We calculate the percentage of each burn severity class (unburned, unburned to low, low, moderate, high, increased greenness) comprising 1 km SSEBop pixels and retain the fractional data for each pixel. Similarly, we calculate the percentage of each pre-fire National Land Cover Database (NLCD) vegetation cover type comprising each SSEBop pixel. The date of a pixel's fire determines which NLCD raster to use (2004, 2006, 2008, 2011, 2013, using the raster most recently preceding the fire event) (Wickham et al., 2014).

Monthly air temperature data are extracted at each SSEBop pixel from 4 km PRISM rasters and the maximum monthly temperature (averaged over all days in the month) for all years 2000 through 2015 is calculated (Oregon State University, Northwest Alliance for Computational Science and Engineering, 2019). The area-weighted average is used when a 1 km SSEBop pixel intersects more than one 4 km PRISM pixel. Daily SNOw Data Assimilation (SNODAS) 1 km SWE rasters (National Operational Hydrologic Remote Sensing Center, 2004) are filtered to the last day of each of the winter months (December through February) and the mean of the final monthly SWE is calculated for each pixel. SWE and air temperature data are not normalized in the current study and are therefore dependent on climate and location. To account for pre-fire antecedent soil moisture, the average Palmer Drought Severity Index (PDI) score for the 12 months preceding the fire is calculated from 2.5 degree monthly rasters (Dai, 2017). Latitude and longitude are the centroid of each 1 km SSEBop pixel.

Elevation, aspect, and slope were obtained from 30 m Landfire rasters and upscaled to 1 km (USDA Forest Service, USDI, n.d.). To upscale aspect, we use a procedure to account for the discontinuity at zero/360 degrees (Pewsey, 2014). Measures of eastness and westness are generated at each pixel by converting degrees to radians and taking the difference of the sine and cosine of each radian from its arctangent. Potential direct incident solar radiation is calculated from aspect, slope, and latitude using an equation provided by McCune and Koen (2002). Gridded available water capacity (AWC) data (provided as cm water per cm of soil) were obtained from the Gridded National Soil Survey Geographic Database (gNATSGO) (USDA NRCS, n.d.). The spatial resolution of the native gNATSGO file is variable; the area-weighted average is used when more than one soil class polygon intersects the 1 km SSEBop grid. Lithologic data of variable spatial resolution were obtained from the State Geological Map compilation (Horton, 2017) and the fraction of each SSEBop pixel underlain by igneous, sedimentary, metamorphic, or unconsolidated parent material calculated.

2.2. ET_a response metrics

Metrics to capture the post-fire ET_a response are calculated at each pixel for each post-fire year one through five. To normalize for precipitation variability across the CONUS, evaporation ratios (ET/P) are also calculated at each 1 km pixel with monthly 4 km PRISM precipitation data using an area-weighted average if the 1 km grid intersects more than one PRISM cell (Oregon State University, Northwest Alliance for Computational Science and Engineering, 2019). Percent and magnitude ET_a and ET/P change between each post-fire year and the pre-fire five-year average ET_a and ET/P are calculated. Pre-fire average annual ET_a and ET/P are the average annual ET_a depth and evaporation ratio for the five years preceding the month of fire ignition; post-fire year one ET_a and ET/P are the total ET_a and ET/P for the 12 months following the fire event, starting one month after the fire ignition month (according to the date of fire ignition as recorded in the MTBS database). Post-fire year two is the next 12-month interval, and so on. For example, if a fire ignited on July 15, 2010, post-fire year one is September 1, 2010 through August 31, 2011. Using a burn time between one to two months aligns with Westerling's (2016) finding that from 2003 to 2012, the mean burn time in the western US was 52 days (Westerling, 2016).

SSEBop may overestimate ET_a from unvegetated areas because algorithms used to process reflectivity data can underestimate the LSTs of high albedo surfaces (McShane et al., 2017). Areas of higher and lower precipitation and ET_a may also be underrepresented in the lower resolution PRISM precipitation data compared to the finer resolution SSEBop ET_a data. Using relative pre and post-fire differences allows even the pixels with unusually high ET/P ratios to provide meaningful information. For example, even the pixel with the highest pre-fire average ET/P included in the analysis (a shrubby area in Arizona) has a post-fire year one percent change of only −15% because the post-fire year one ET/P ratio is as similarly inflated as the pre-fire average ET/P ratio.

2.3. ET_a recovery metrics

Metrics to assess ET/P recovery over time are calculated following Pickell et al. (2016) and Frazier et al. (2018). For each pixel, the Relative Recovery Indicator (RRI), the Ratio of 80% Pre-disturbance (R80P), and the Year-on-Year Average (YrYr) are computed using the magnitude change in ET/P. RRI takes the maximum ET/P value from post-fire year four or five and compares it to the initial, post-fire year one ET/P value (equation (1)). Negative values indicate reductions in ET/P over time relative to initial disturbance, zero indicates no recovery, a value of one indicates an equal amount of recovery relative to initial disturbance, and positive values indicate gains in ET/P over time.

$$RRI = \frac{\max\left(ETP_{post4}, ETP_{post5}\right) - ETP_{post1}}{pre_{ave_{ETP}} - ETP_{post1}} \quad (1)$$

R80P is the percent recovered back to 80% of the pre-fire average ET/P by year four or five (equation (2)). Interpretation is similar to RRI's. Negative values indicate ET/Ps smaller than 80% of pre-fire ET/P by post-fire year four or five, one indicates recovery equivalent to 80% of pre-disturbance values, and values greater than one exceed 80% of pre-disturbance ET/P.

$$R80P = \frac{\max\left(ETP_{post4}, ETP_{post5}\right)}{\left(pre_{ave_{ETP}}\right)*0.8} \quad (2)$$

YrYr is the average annual post-disturbance change in the first five post-fire years (equation (3)). Negative values indicate an average loss in ET/P each year, zero indicates no recovery, and positive values indicate an average gain, or recovery, in ET/P each year (Frazier et al., 2018).

$$YrYr = \frac{\max\left(ETP_{post4}, ETP_{post5}\right) - ETP_{post1}}{5} \quad (3)$$

2.4. K-means clustering

K-means clustering (MacQueen, 1967) is used to segment burned CONUS SSEBop pixels into related groups according to the direction and magnitude of ET/P response in post-fire year one (Fig. 2, Fig. 3). ET_a is not included in the clustering analysis because it does not normalize for the climatic variability present in the CONUS. K-means clustering is a heuristic, unsupervised ML algorithm that separates *n* observations into

Table 1
Summary of the parent datasets and calculated response and recovery metrics used in study. Table provides the name of dataset or metric, source of the dataset, native spatial and temporal resolution, units, and data processing steps.

	Data/Variable Name	Abbreviation	Data Source	Native Spatial Resolution	Native Temporal Resolution	Modified Temporal Resolution	Unit	Processing
Response variables	Actual evapotranspiration	ET_a	SSEBop, USGS (Senay et al., 2007, 2013)	1 km	Monthly	–	Depth (mm)	Projection transformed to CRS Albers Equal Area NAD83
	Evapotranspiration ratio	*pre_ave_ET/P* and *ET/P_postX* (year one through five)	Calculated from ET_a and *ppt*	1 km	Monthly	Annual	Fraction (mm/ mm)	Calculated on an annual basis from monthly SSEBop ET_a and PRISM ppt depths. *pre_ave_ET/P* is the average ET/P for the 60 months (five years) prior to the month fire was ignited; *ET/P_postX* (one through five) are the first twelve months beginning one month after month of fire ignition (post-fire year one), second twelve months following post-fire year one (post-fire year two), etc.
	Percent change in ET/P in post-fire years 1 through 5	*pc_ET/P_yrX* (year one through five)	Calculated from *pre_ave_ET/P* and *ET/P_postX*	1 km	Annual	–	Percent	Percent change calculated from each *ET/P_postX* value (years one through five) relative to *pre_ave_ET/P*
	Magnitude change in ET/P in post-fire years 1 through 5	*abs_yrX_ET/P* (year one through five)	Calculated from *pre_ave_ET/P* and *ET/P_postX*	1 km	Annual	–	Fraction	Magnitude change (difference) calculated from each *ET/P_postX* value (years one through five) relative to *pre_ave_ET/P*
Recovery metrics	Relative recovery indicator	*RRI*	Calculated from *abs_yrX_ET/P*	1 km	Annual	–	Fraction	From Frazier et al. (2018), *RRI* calculated from *pre_ave_ET/P* and *ET/P_postX* as the percent recovery of ET/P by post-fire year four or five, whichever is greatest, relative to the initial magnitude change in ET/P (max(*ET/P_post4*, *ET/P_post5*)/ (*pre_ave_ET/P* - *abs_yr1_ET/P*))
	Ratio 80% of Pre-disturbance	*R80P*	Calculated from *abs_yrX_ET/P*	1 km	Annual	–	Fraction (converted to percent in Fig. 10)	From Frazier et al. (2018), *R80I* calculated from *pre_ave_ET/P* and *ET/P_postX* as the percent recovery of ET/P by post-fire year four or five, whichever is greatest, relative to the 80% of the pre-disturbance value (max(*ET/P_post4*,

(*continued on next page*)

Table 1 (*continued*)

	Data/Variable Name	Abbreviation	Data Source	Native Spatial Resolution	Native Temporal Resolution	Modified Temporal Resolution	Unit	Processing
								ET/P_post5)/(0.8* *pre_ave_ET/P*))
	Year-on-year average	*YrYr*	Calculated from *abs_yrX_ET/P*	1 km	Annual	–	Fraction (converted to percent in Fig. 10)	From Frazier et al. (2018), *YrYr* calculated from *ET/P_postX* as the average percent recovery of ET/P experienced each post-fire year (max (*ET/P_post4, ET/P_post5*)) – ((*ET/P_post1)*/5)
Independent variables	Burn severity	*burnsev_low_percent* *burnsev_mod_percent* *burnsev_high_percent*	Calculated from MTBS dNBR raster (Eidenshink et al., 2007)	30 m	Compiled annually for each MTBS-mapped fire	–	Percent	Percent of each 1 km SSEBop pixel comprised by each burn severity class (calculated)
	Land cover	*nlcdXX_percent*	Calculated from most recent pre-fire NLCD land cover raster (2001, 2004, 2006, 2008, 2011, 2013, 2016) (Wickham et al., 2014)	30 m	Static	–	Fraction	Fraction of each 1 km SSEBop pixel comprised by each NLCD class (calculated)
	Precipitation	*ppt*	Parameter-elevation Regressions on Independent Slopes Model (PRISM) (2019) (Oregon State University, Northwest Alliance for Computational Science and Engineering, 2019)	4 km	Monthly	Annual	Depth (mm)	- Downscaled from 4 km to 1 km using area-weighted average when more than one PRISM tile underlaid SSEBop pixel - Monthly total precipitation depths (rain + melted snow) summed to annual
	Temperature, maximum monthly	*tmax*	PRISM (2019) (Oregon State University, Northwest Alliance for Computational Science and Engineering, 2019)	4 km	Monthly	Annual	Degrees (C)	- Downscaled from 4 km to 1 km using area-weighted average when more than one PRISM tile underlaid SSEBop pixel - Maximum monthly temperature (averaged over all days in the month) averaged over years 2000–2015
	Snow-water equivalent	*SWE*	NOAA National Operational Hydrologic Remote Sensing Center (NOHRSC) Snow Data Assimilation System (SNODAS) (National Operational Hydrologic Remote Sensing Center, 2004)	1 km	Daily	Mean monthly depth for winter months only	Depth (mm)	Average end-of-month SWE depth for winter months (December through February)
	Palmer Drought Severity Index	*PDI*	NOAA, UCAR/ NCAR, Western Regional Climate Center, Dai Global PDSI (Dai, 2017)	2.5 degree	Monthly	Average score for the twelve months preceding the fire ignition month	Score (-10 = most severe dryness, +10 = most severe wetness)	- Downscaled from 2.5 degree to 1 km using area-weighted average when more than one PDI tile underlaid SSEBop pixel - Calculated average score for

(*continued on next page*)

Table 1 (*continued*)

Data/Variable Name	Abbreviation	Data Source	Native Spatial Resolution	Native Temporal Resolution	Modified Temporal Resolution	Unit	Processing
							twelve months preceding fire ignition month
Available Water Capacity	*AWC*	USDA-NRCS Gridded National Soil Survey Geographic Database (gNATSGO) (USDA NRCS, n.d.)	Variable	Static. Compilation of best available soils data from STATSGO2, SSURGO, and Raster Soil Surveys	–	Cm water per cm soil per km, 0–91 cm. The available water supply multiplied by thickness of soil	Downscaled from variable spatial resolution to 1 km using area-weighted average when more than one soil class polygon underlaid SSEBop pixel
Latitude	*latitude*	Centroid of SSEBop pixel	–	Static	–	Degrees, minutes, seconds	Centroid of SSEBop pixel extracted from SSEBop raster
Longitude	*longitude*	Centroid of SSEBop pixel	–	Static	–	Degrees, minutes, seconds	Centroid of SSEBop pixel extracted from SSEBop raster
Elevation	*elevation*	Landfire (USDA Forest Service, USDI, n.d.)	30 m	Static	–	Meter	Upscaled to 1 km using area-weighted average
Slope	*slope*	Landfire (USDA Forest Service, USDI, n.d.)	30 m	Static	–	Degrees	Upscaled to 1 km using area-weighted average
Potential direct incident solar radiation	*solarrad_1*	Calculated from slope, aspect, latitude (McCune and Keon, 2002). Slope, aspect, latitude from Landfire (USDA Forest Service, USDI, n.d.)	30 m	Static	–	MJ cm-2 yr-1	Upscaled to 1 km using area-weighted average for slope and latitude, arctan-1 (cos(rad), sin(rad)) of aspect
Lithology (fraction sedimentary, igneous, metamorphic, unconsolidated)	*frac_sed* *frac_ign* *frac_meta* *frac_unc*	State Geological Map Compilation (Horton, 2017)	State USGS geological maps ranging in scale from 1:50,000 to 1:1,000,000	Static	–	Fraction	Downscaled from variable spatial resolution to 1 km using area-weighted average when more than one polygon underlaid SSEBop pixel. Provided as the fraction of each 1 km SSEBop pixel comprised by sedimentary, igneous, metamorphic, and unconsolidated data class (calculated)

k clusters, where *k* is pre-specified by the analyst. Observations (pixels) are grouped such that cluster members are as similar (cohesive) to each other and as dissimilar (separated) to the other clusters as possible according to their sum of squared error (Lee et al., 2011; MacQueen, 1967). The k-means base R function is used with an nstart of 25 and no limit on the maximum number of iterations allowed. The silhouette score is calculated with the base R silhouette function to determine the appropriate number of clusters (*k*). Silhouette values indicate the aggregate similarity of data points within the same cluster relative to the members of other clusters (Rousseeuw, 1987). Explanatory variables are excluded from the clustering algorithm to reduce spatial biases inherent to topographic, geologic, and climatic characteristics. Parametric one-way analysis of variance (ANOVAs) t-tests and Tukey's honestly significant difference (HSD) single-step multiple comparison tests are run on cluster groups to ensure response metrics are significantly different ($\alpha = 0.05$) between the resultant clusters (Rouder et al., 2016).

Unsupervised partitioning can yield less predictable results than supervised learning methods and precise information about the algorithm's data sorting methods is not provided (Battaglia et al., 2016). This makes it difficult to understand the underlying relationships differentiating the resulting cluster groups and limits the knowledge gained from the analysis about post-fire processes. To address these limitations, clusters are separated further into pre-defined Environmental Protection Agency (EPA) Level I Ecoregions (Omernik and Griffith, 2014). Relationships between ET/P response and independent variables are explored within each unique cluster-EPA ecoregion group (discussed in the following section).

2.5. Evaluation of controlling factors and their spatial patterns

Distributions of independent variables between clusters are visualized with boxplots (SM Figure B). However, due to the high ecologic, topographic, and climatic variability present in the CONUS, we hypothesize that relationships between post-fire ET/P response and independent variables may be regionally unique. If so, this would limit our ability to identify controlling relationships from CONUS-scale data

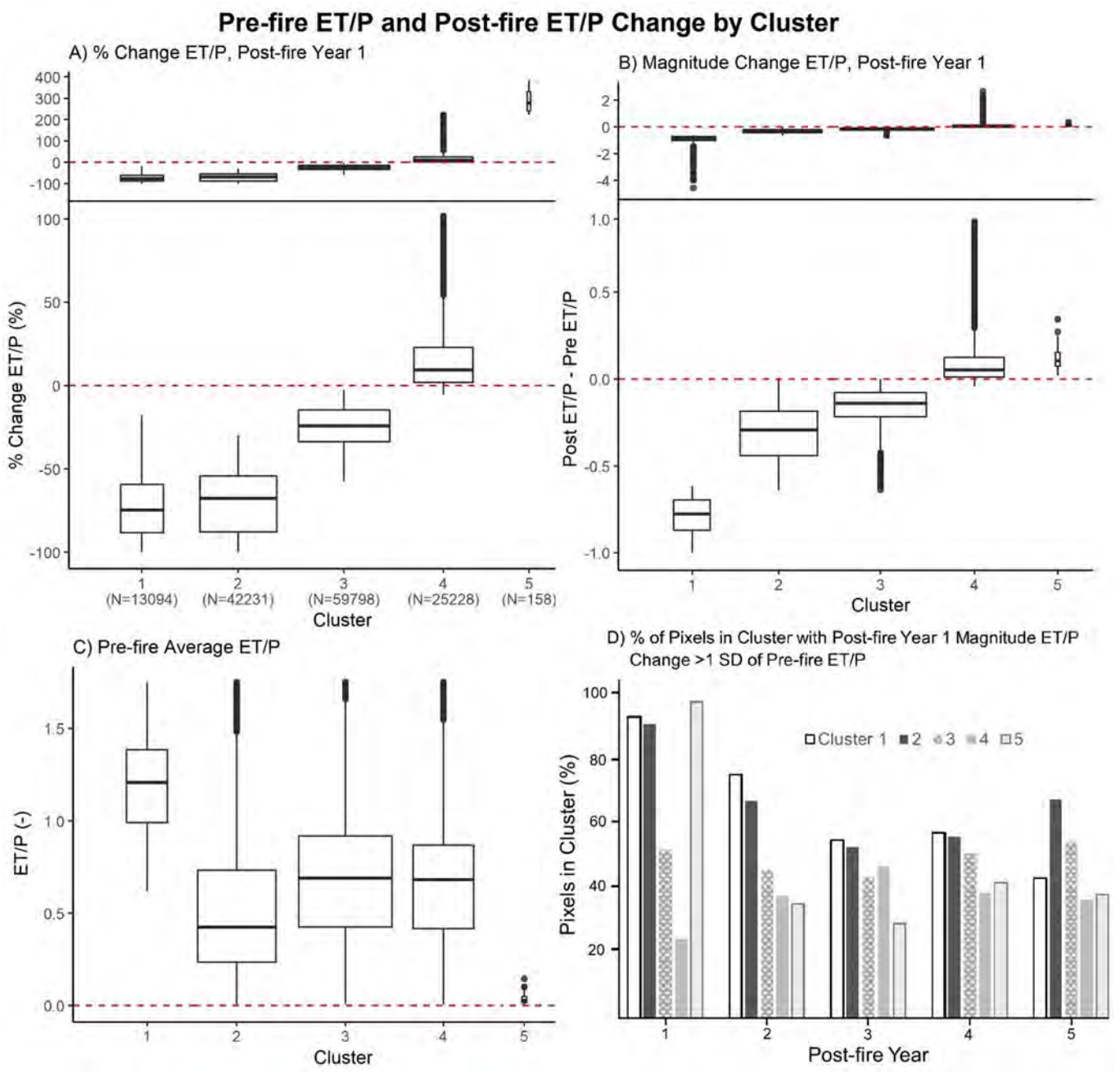

Fig. 2. Statistical distribution of SSEBop pixels between clusters (response groups). Boxplot center bars indicate median, boxplot hinges are 25th and 75th percentiles, and whiskers are the largest value less than 1.5*interquartile range (IQR) ± each hinge. Outliers are plotted as individual points. Box widths indicate sample size. Percent and magnitude changes in post-fire ET/P are calculated from mean pre-fire ET/P. Zero change from the pre-fire mean ET/P is indicated by the dashed horizontal red line. (A) Boxplots of post-fire year one percent change in ET/P for each of the five clusters (number of pixels in cluster provided below x-axis label). Plots provided at two different y-scales to show the large percentage increase in cluster 5 (y-axis scale extended to 400% in top plot). (B) Boxplots of post-fire year one magnitude change in ET/P for each of the five clusters. Plots provided at two different y-scales to show the large magnitude decrease in cluster 1 (y-axis scale extended to −400% in top plot) and large magnitude increase in cluster 4 (y-axis scale extended to 200% in top plot). (C) Pre-fire five-year average ET/P of each cluster. (D) Percent of pixels in each cluster with magnitude changes in ET/P greater than one standard deviation of their five-year pre-fire ET/P values. Shown for post-fire years one through five (x-axis). For example, in post-fire year one, 95% of cluster one's pixels have a magnitude change in ET/P greater than the pre-fire ET/P variability (represented by an exceedance of one standard deviation of the fire pre-fire annual ET/P values), whereas only approximately 25% of cluster 4's pixels exceed pre-fire ET/P standard variability. (For interpretation of the references to color in this figure legend, the reader is referred to the web version of this article.)

summaries or analyses. To gain insight, after pixels are grouped into clusters, pixels are further separated into EPA Level I Ecoregions (EPA ecoregion) (Fig. 4). The EPA uses physical and biological spatial correlation patterns to divide North America into regions that are generally similar in terms of the type, quality, and quantity of environmental resources. Although regions mapped at coarser resolution have greater underlying variability within each ecoregion, we use the Level I delineation because of the broad spatial extent of our study.

The average of each independent variable is calculated for each unique EPA ecoregion-cluster data subset (SM Table B). The resultant data summary is a geophysical description of each EPA ecoregions' burned areas and provides a qualitative snapshot of regional patterns between potentially explanatory variables and post-fire ET/P response (using cluster assignment as a proxy for response). Patterns are indeed

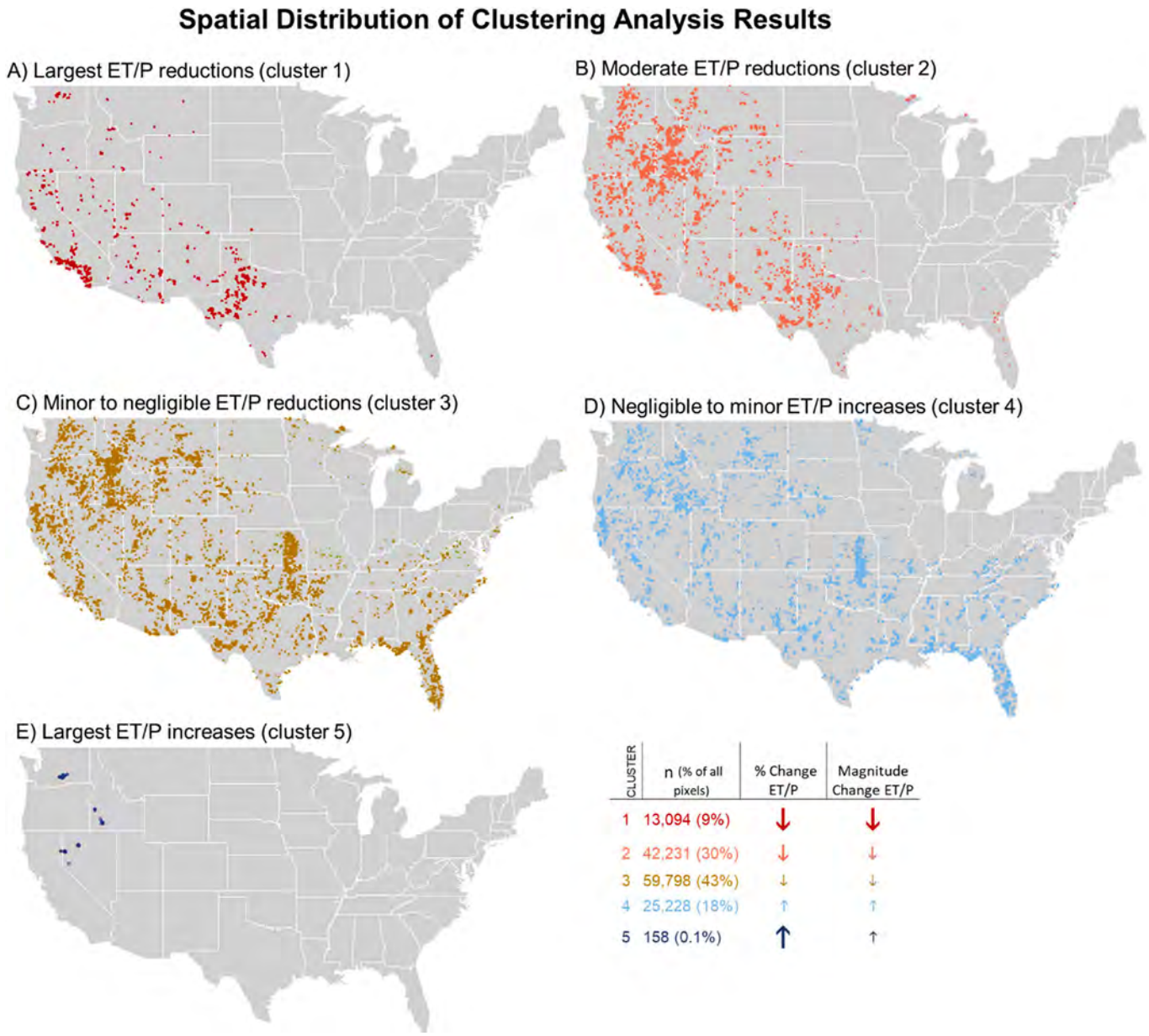

Fig. 3. Spatial distribution of all burned SSEBop pixels included in the study by cluster. Table includes the number of pixels per cluster (n) and as a percentage of total pixels and the general trend of percent and magnitude ET/P change in post-fire year one. Trend is indicated by direction and size of arrow (down indicates post-fire ET/P reduction).

spatially variable, forming the basis for conducting quantitative statistical testing on both CONUS and regional-scale datasets (to test for overarching trends). Summaries of incident type (prescribed versus wildfire), post-fire ET/P response, and location can now be generated at different spatial scales.

Pearson's R correlation is evaluated between independent variables and the percent change in ET/P in post-fire year one in R. The analysis is repeated on various data subsets including a) all 140,509 CONUS pixels, b) pixels in each cluster (e.g., all pixels in the CONUS assigned to cluster 2), c) pixels in each EPA Level I ecoregion (e.g., all pixels within the Eastern Temperate Forests EPA ecoregion, regardless of cluster assignment), and d) pixels in each unique combination of cluster assignment and EPA Level I ecoregion (e.g., pixels assigned to cluster 2 within the Eastern Temperate Forests EPA ecoregion). Statistical significance of correlation measures is evaluated with Pearson's method from the *Kendall* R package ($\alpha = 0.05$) (McLeod, 2011).

A multiple linear regression (MLR) least-squares model is constructed for each data subset to evaluate the relative importance of explanatory variables on post-fire year one ET/P percent change. The absolute value of an explanatory variable's regression coefficient describes how much response variance is accounted for by the dependent variable (Farmer et al., 2019). The MLR model R^2 describes the degree to which response variance is accounted for by all of the independent variables included in the model collectively (Davis, 2002). Only independent variables that are significantly correlated with ET/P response ($p \leq 0.05$, $R \geq 0.20$) are included in each data subset's MLR model, and only the variable with the higher R value is retained when explanatory variables are collinear. Regression models are constructed in R, and regression coefficients are standardized with the *QuantPsyc* package's lm.beta function (Fletcher, 2012).

2.5.1. Burn scar scale assessment

To further test the effect of scale on the explanatory power of independent variables, correlation is evaluated and MLR models constructed

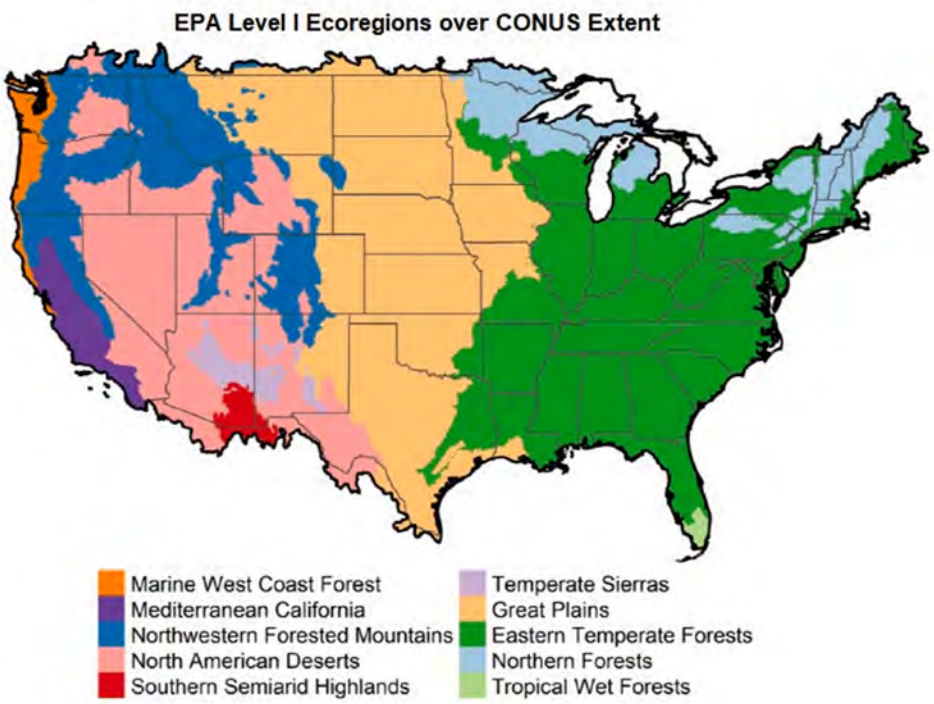

Fig. 4. Distribution of the ten EPA Level I Ecoregions covering the CONUS study domain (Omernik and Griffith, 2014).

for pixels within three individual fires (2007 Zaca Fire in southern California (Fig. 5); 2012 High Park Fire in the Colorado Rocky Mountains (Fig. 6); 2013 Rim Fire on the western slope of California's Sierra Nevada (Fig. 7)). The fires are randomly selected such that different parts of the CONUS and the range of ET/P responses (pixels assigned to clusters 1 through 4) are sampled.

2.6. Attribution of ET/P shift to fire

The standard deviation of each pixel's annual ET/P data for the five years preceding the fire is calculated and compared to the magnitude change in post-fire year one ET/P. A difference-in-difference (DID) regression is also used to compare pre and post-fire ET/P time series from pairs of burned and unburned pixels from a selection of fires in the western US. DID is frequently used in econometrics to determine the effect of a treatment on outcome (response). One group is exposed to the treatment, one is not, and the difference in the outcome variable is tracked before and after exposure. The untreated group controls for confounding factors that simultaneously influence response (Müller and Levy, 2019). In the DID analysis, burned pixels assigned to cluster 1 are the treatment group and pixels from adjacent, unburned areas are the control. Cluster 1 pixels are used because their relatively large post-fire year one ET/P reductions make them more likely to exhibit behavior that can be differentiated from signals in the climate data (Hallema et al., 2018; Lau and Weng, 1995).

2.6.1. Pixel selection

Due to computational limits, only a subset of the 140,509 burned SSEBop pixels included in the greater study are evaluated with the DID analysis. To test a range of conditions, one fire is randomly selected from each of the four EPA ecoregions containing the majority of cluster 1 pixels (Northwestern Forested Mountains, Great Plains, North American Deserts, Mediterranean California (pixel counts provided in SM Table C)). Both fires from the burn scar scale analysis with pixels assigned to cluster 1 (Rim Fire, Zaca Fire) are also included in the DID analysis for continuity. At each of the six fires, ten pixels from adjacent, unburned areas are randomly selected from nearby locations with similar pre-fire vegetation and topography to the burned areas. We evaluate ten pixels from each fire so that a range of local conditions and proximities (distance from the burned area) can be tested. All pixels are located at least 1 km away from the burn perimeter but do not exceed a distance greater than the length of the burned area's longest radius. The majority are within 4 km of the burn perimeter (the length of a 4 km PRISM cell) and within a 12-digit hydrologic unit (https://water.usgs.gov/GIS/huc.html) that intersects the burn scar (following Ma et al. (2020)). The annual pre and post-fire ET/P ratio is calculated for each unburned pixel. Unburned pixels are paired with the cluster 1 pixel from the adjacent burned area with the most similar pre-fire ET/P behavior according to the root mean square error (RMSE) of their annual ET/P time series for the five years preceding the fire.

2.6.2. DID and change point analyses

DID linear regression models are constructed for each pixel pair in R using pre and post-fire annual ET/P as the response variable and dummy variables to represent pre and post-fire periods and treatment and control groups. Due to the small sample size of each pair (five annual pre-fire data points, between two and five post-fire annual data points depending on the date of the fire), p-values ≤ 0.10 are considered statistically significant.

Non-parametric Pettitt's change point detection tests are applied to each burned pixels' annual ET/P time series to independently check the timing of major behavioral shifts (Mallakpour and Villarini, 2016; Zhou et al., 2019). Pettitt's is based on the Mann-Whitney two-sample rank-based test and detects a single change at an unknown point in time; it is among the most widely used change point detection methods in hydroclimatological studies (Mallakpour and Villarini, 2016; Zhou et al., 2019). Pettitt's is applied with the pettitt.test function from the *trend* package in R (Pohlert, 2020). Due to the small sample size, p-values ≤ 0.10 are considered statistically significant.

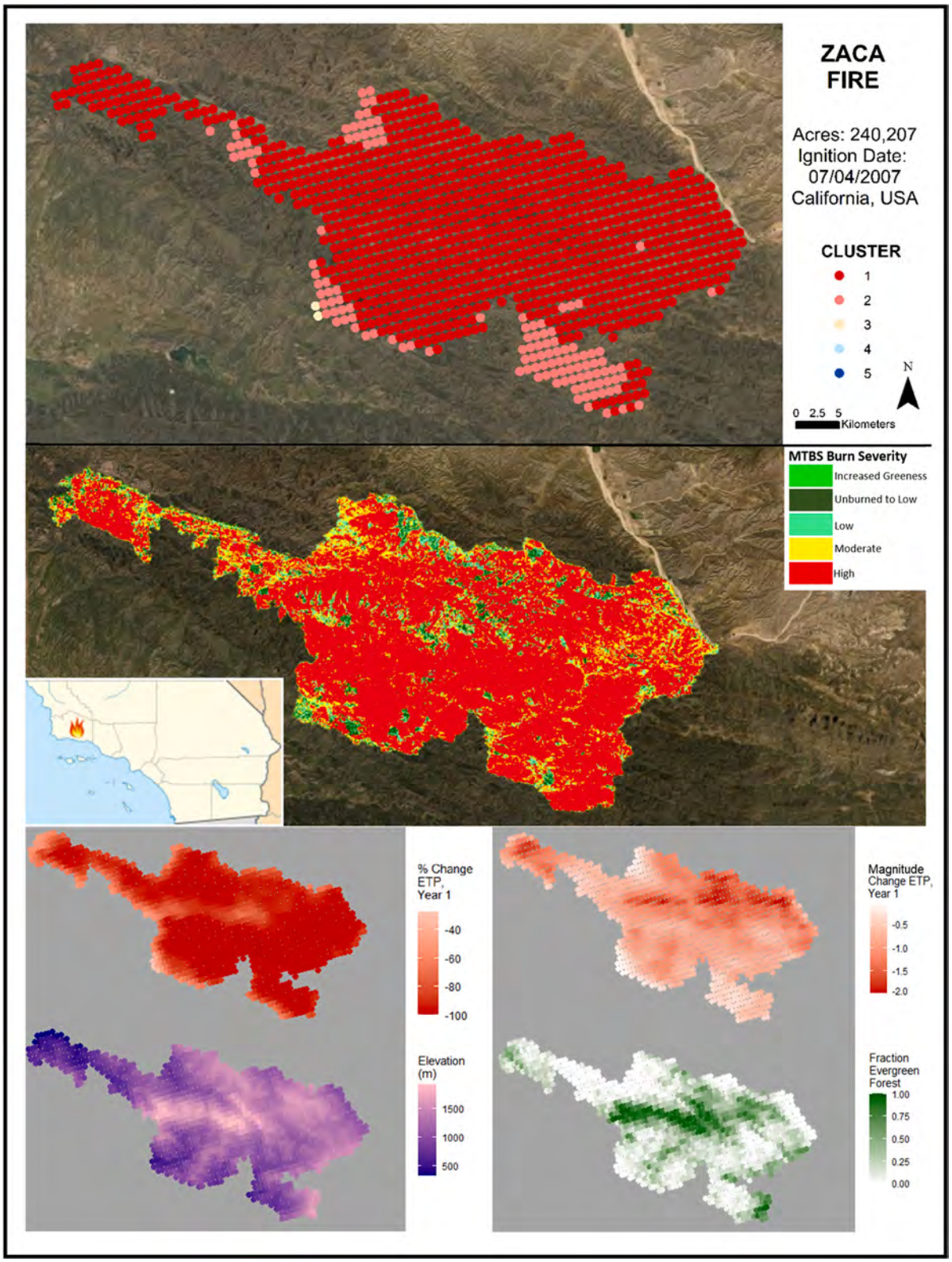

Fig. 5. Zaca Fire [CA34695119659200707O4], Santa Barbara County, southern California, US, ignited July 4, 2007. (TOP) Cluster assignment of SSEBop pixels (data plotted at the centroid of the pixel) included in fire perimeter and clustering analysis (percentage of SSEBop pixel burned has to be ≥75% to be retained for analysis); (MIDDLE) MTBS burn severity rating and percent and magnitude change in ET/P in post-fire year one; (BOTTOM) percent change and magnitude change in ET/P in post-fire year one, elevation (m), and the fraction of evergreen forest (NLCD class 42) comprising each pixel (the latter has one of the strongest correlations with post-fire year one percent change ET/P (Table 3)). Legend scales indicate the maximum and minimum range of values for each metric for pixels in the fire. Basemapping imagery from ArcMap v10.8. Service layer credits include "Esri, DigitalGlobe, GeoEye, Earthstart Geographics, CNES/Airbus DS, USDA, USGS, AeroGRID, IGN, and the GIS User Community."

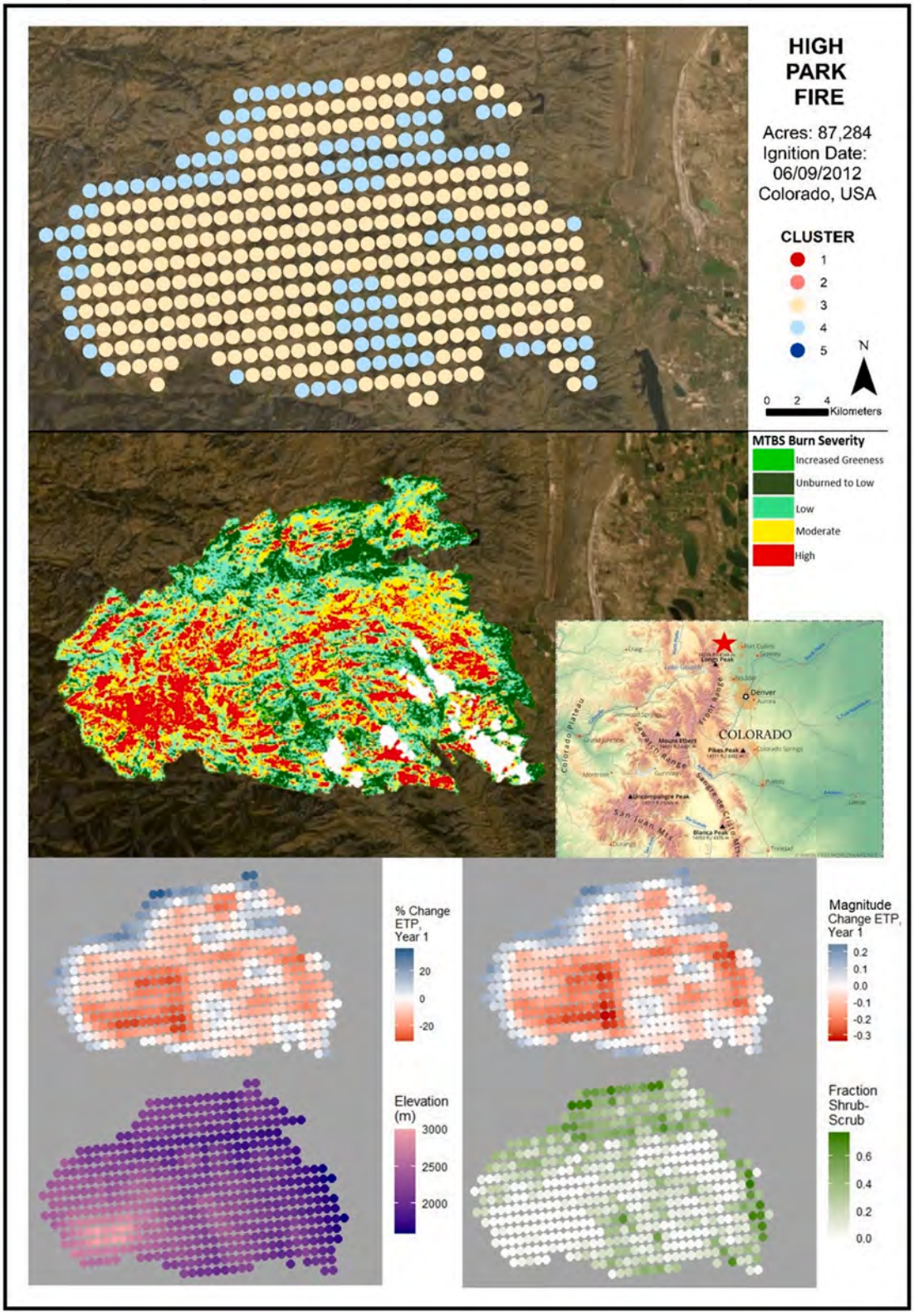

Fig. 6. High Park Fire [CO40589105404201206O9], Larimer County, Colorado, US, ignited June 9, 2012. (TOP) Cluster assignment of SSEBop pixels (data plotted at the centroid of the pixel) included in fire perimeter and clustering analysis (percentage of SSEBop pixel burned had to be ≥75% to be retained for analysis); (MIDDLE) MTBS burn severity rating and percent and magnitude change in ET/P in post-fire year one; (BOTTOM) percent change and magnitude change in ET/P in post-fire year one, elevation (m), and the fraction of shrub/scrub cover (NLCD class 52) comprising each pixel (the latter has one of the strongest correlations with post-fire year one percent change ET/P (Table 3)). Legend scales indicate the maximum and minimum range of values for each metric for pixels in the fire. Basemapping imagery from ArcMap v10.8. Service layer credits include "Esri, DigitalGlobe, GeoEye, Earthstart Geographics, CNES/Airbus DS, USDA, USGS, AeroGRID, IGN, and the GIS User Community."

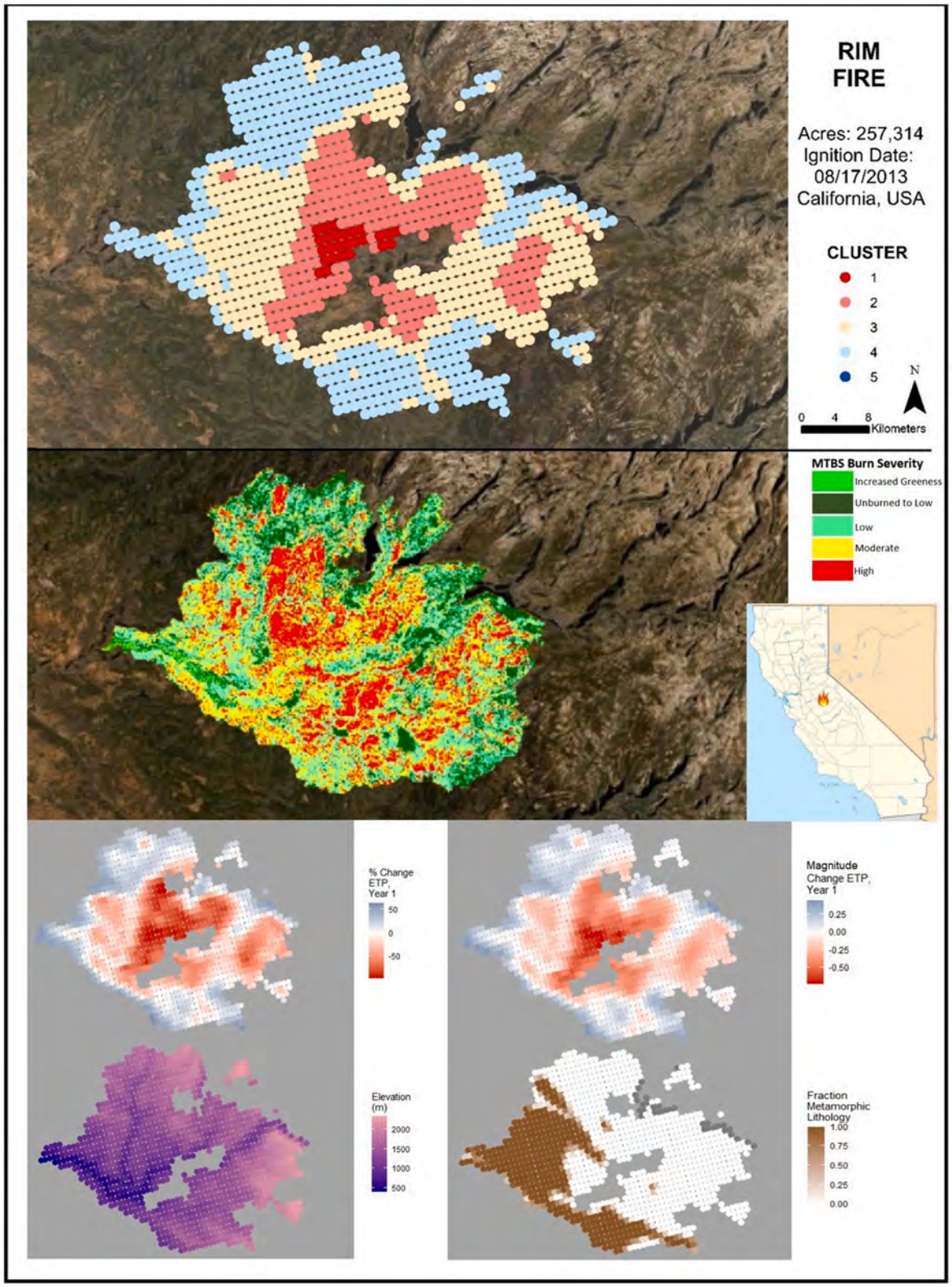

Fig. 7. Rim Fire [CA37857120086201308 17], Stanislaus National Forest, California, US, ignited August 17, 2013. (TOP) Cluster assignment of SSEBop pixels (data plotted at the centroid of the pixel) included in fire perimeter and clustering analysis (percentage of SSEBop pixel burned had to be ≥75% to be retained for analysis); (MIDDLE) MTBS burn severity rating and percent and magnitude change in ET/P in post-fire year one; (BOTTOM) percent change and magnitude change in ET/P in post-fire year one, elevation (m), and the fraction of metamorphic lithology comprising each pixel (the latter has one of the strongest correlations with post-fire year one percent change ET/P (Table 3)). Legend scales indicate the maximum and minimum range of values for each metric for pixels in the fire. Basemapping imagery from ArcMap v10.8. Service layer credits include "Esri, DigitalGlobe, GeoEye, Earthstart Geographics, CNES/Airbus DS, USDA, USGS, AeroGRID, IGN, and the GIS User Community."

3. Results

3.1. Spatial and temporal ET/P response

3.1.1. Initial post-fire ET/P response

CONUS-scale maps indicate that the dominant response of ET_a and ET/P to fire is a reduction in the first post-fire year (Fig. 1C through F). The largest magnitude reductions occur in the southwest, while pixels in the northwest have the lowest pre-fire average ET/Ps (Fig. 1B) which makes them susceptible to large percent changes from comparatively small magnitude shifts in ET/P. Pre-fire annual ET_a is highest in the southeast US and portions of northern California and the Pacific Northwest that receive high annual precipitation (Fig. 1A). Post-fire ET_a changes mimic post-fire ET/P changes spatially (Fig. 1C and E).

To identify super-regional to CONUS-scale response patterns, pixels are grouped into five clusters following results from the silhouette score analysis. ET/P is reduced in 82% of all pixels analyzed during the first post-fire year (Fig. 2, Fig. 3) including in all pixels assigned to clusters 1, 2, and 3. Cluster 1 comprises 9% of the pixels evaluated (Fig. 2, Fig. 3). Its members are characterized by the largest percent change (Fig. 2A) and magnitude (Fig. 2B) ET/P reductions and largest pre-fire average ET/Ps (Fig. 2C). The majority of cluster 1 pixels are located in the southwestern US within the Mediterranean California, Great Plains, North American Deserts, and Northwestern Forested Mountains EPA ecoregions (SM Table C). Of all EPA ecoregions, the biggest average reductions in percent and magnitude post-fire year one ET/P and ET_a occur in the Mediterranean California EPA ecoregion (Table 2).

Cluster 2 comprises 30% of pixels. Relative to pixels in cluster 1, cluster 2 pixels exhibit similarly large percent change ET/P reductions but smaller magnitude ET/P reductions, possibly due to their smaller pre-fire average ET/Ps. The majority of cluster 2 pixels are located in the western US within the North American Deserts, Great Plains, Northwestern Forested Mountains, and Mediterranean California EPA ecoregions (SM Table C). Cluster 3 comprises 43% of pixels. Members are characterized by moderate to negligible post-fire year one percent and magnitude change ET/P reductions and are well-distributed across the CONUS. Cluster 4 comprises 18% of pixels and is characterized by negligible to moderate increases in ET/P in post-fire year one. Like cluster 3, cluster 4 pixels are well-distributed across the CONUS but are most prevalent in the east and southeastern US; nearly all pixels in the eastern US are assigned to cluster 3 or 4. Cluster 5 comprises 0.1% of pixels. All 158 members are in the North American Deserts EPA Ecoregion and have small pre-fire average ET/Ps, which renders them susceptible to large percent changes. They have large percent but small magnitude increases in ET/P in post-fire year one. Tukey HSD pairwise comparisons of ANOVA tests indicate that pre-fire average ET/P ratios and percent and magnitude ET/P changes are statistically different ($p \leq 0.05$) between all clusters in the first post-fire year, except the magnitude change between clusters 4 and 5.

A greater percentage of cluster 4′s pixels are in prescribed burn areas (15%) than any other cluster (cluster 3: 7%; cluster 2: <1%; cluster 1: <1%, cluster 5: 0%). Within cluster 4, pixels in EPA ecoregions located in the eastern CONUS have the highest percentage of pixels in prescribed burns (highest percentage in the Eastern Temperate Forests (63%) followed by Tropical Forests (39%)) (SM Table C). Results are similar for pixels in cluster 3 (highest percentage of prescribed burn pixels are in Tropical Forests (51%) followed by Eastern Temperate Forests (42%)). Of the cluster 1 and 2 pixels, the only EPA ecoregion-cluster combination with prescribed burn pixels comprising >1% of total pixel counts are cluster 2 Eastern Temperate Forest pixels (16%). Thus, as a percentage of total fire activity in each ecoregion, fires are prescribed more frequently in the eastern CONUS than in the west. In addition, cluster 4 pixels have the highest percentage of low burn severity area (except for the 158 pixels in cluster 5) (SM Figure B, SM Table B). These results suggest that prescribed fire tends to yield lower burn severities and smaller ET/P reductions than wildfire.

3.1.2. Inter and intra-fire ET/P response variability

Statistical summaries of initial ET/P response and short-term recovery are provided by EPA ecoregion (Table 2) and US State (SM Table A). According to standard deviations of cluster assignment and the percent and magnitude ET/P change in the first post-fire year, some states and EPA ecoregions have higher inter and potentially intra-fire variability than others. Possibly owing to its greater topographic and climatologic complexity (Hallema et al., 2018), ET/P response is more variable in the western CONUS (where pixels are assigned to all five clusters) than in the east (where nearly every pixel is assigned to clusters 3 or 4) (Fig. 3, Fig. 8). The eastern EPA ecoregions (Tropical Wet Forest and Eastern Temperature Forest) also have the smallest post-fire year one percent ET/P change standard deviations (Table 2). ET/P response is fairly consistent in some parts of the west at both the burn scar and regional scale, such as in southern California where nearly every pixel is assigned to clusters 1 or 2 (Fig. 5, Fig. 8A) and in the wetter northern California coast ranges where nearly every pixel is assigned to clusters 3 or 4 (Fig. 8F). But where landforms are complex and climatologic and topographic gradients steep, even intra-fire variability can be high (e.g., pixels in the Sierra Nevada's Rim Fire are assigned to clusters 1, 2, 3, and 4 (Fig. 7)).

3.1.3. ET/P recovery over time

Post-fire ET/P approaches pre-fire ET/P with increasing time since fire (Fig. 9). However, in pixels with the greatest initial reductions

Table 2
Summary statistics by EPA Level I Ecoregion for SSEBop pixels included in clustering analysis (filter applied requires at least 75% of a pixel to be burned). Percent and magnitude change in ET/P during the first post-fire year, RRI, R80P, and YrYr recovery metrics, mode and standard deviation of cluster assignment as a measure of spread (variability) of ET/P response in each region, number of fires, the average number of SSEBop pixels per fire, and pre-fire average ET/P. Cell color indicates the magnitude of the cell value. For columns "Percent Change ET/P, Post-fire Year 1," "Magnitude Change ET/P, Post-fire Year 1," and "Magnitude Change ET, Post-fire Year 1," redder hues indicate a reduction in the post-fire year one summary statistic, bluer hues indicate an increase in the post-fire year one summary statistic.

	Cluster		# Fires	# 1 km² SSEBop Pixels per Fire	Pre-fire Mean ET	Pre-fire Mean ET/P	Percent Change ET/P, Post-fire Year 1					Magnitude Change ET/P, Post-fire Year 1					Magnitude Change ET, Post-fire Year 1		RRI	R80P	YrYr
EPA Level I Ecoregion	MODE	SD	SUM	MEAN	MEAN (mm)	MEAN (fraction)	MEAN (%)	MEDIAN (%)	SD	25th Percentile (%)	75th Percentile (%)	MEAN (fraction)	MEDIAN (fraction)	SD	25th Percentile (fraction)	75th Percentile (fraction)	MEAN (mm)	MEDIAN (mm)	MEAN (fraction)	MEAN (fraction)	MEAN (fraction)
5 Northern Forests	3	0.69	55	25	489	0.73	-31	-36	25	-48	-12	-0.23	-0.26	0.21	-0.38	-0.07	-112	-83	0.78	1.18	0.04
6 NW Forested Mountains	3	0.73	786	52	465	0.59	-34	-34	29	-54	-15	-0.19	-0.16	0.20	-0.29	-0.07	-163	-148	-0.12	1.06	0.03
7 Marine West Coast Forests	4	0.52	19	14	852	0.66	8	10	24	-7	28	0.05	0.04	0.18	-0.04	0.19	-97	-90	0.88	1.52	0.02
8 Eastern Temp. Forests	3	0.59	1973	5	1088	0.88	-6	-10	21	-21	5	-0.07	-0.08	0.22	-0.18	-0.04	-54	-24	1.45	1.30	0.02
9 Great Plains	3	0.94	1269	23	520	0.88	-23	-20	30	-43	-4	-0.23	-0.15	0.32	-0.39	-0.03	-157	-95	-0.82	1.32	0.05
10 North American Deserts	2	0.80	871	43	156	0.43	-47	-57	58	-86	-25	-0.20	-0.15	0.41	-0.27	-0.06	-82	-54	2.12	1.69	0.05
11 Mediterranean California	1	0.86	194	48	451	1.00	-70	-80	32	-93	-55	-0.69	-0.67	0.48	-0.99	-0.35	-318	-320	0.83	0.95	0.10
12 Southern Semi-arid Highlands	3	0.80	78	32	447	0.96	-29	-31	25	-46	-16	-0.29	-0.27	0.25	-0.47	-0.13	-156	-142	-0.43	1.24	0.05
13 Temperate Sierras	3	0.79	180	45	524	1.02	-26	-28	24	-41	-15	-0.28	-0.27	0.27	-0.43	-0.13	-161	-163	4.10	1.19	0.02
15 Tropical Wet Forests	3	0.53	93	10	1278	0.98	-4	-6	15	-14	5	-0.06	-0.06	0.16	-0.13	0.04	1	8	-2.26	1.35	0.03

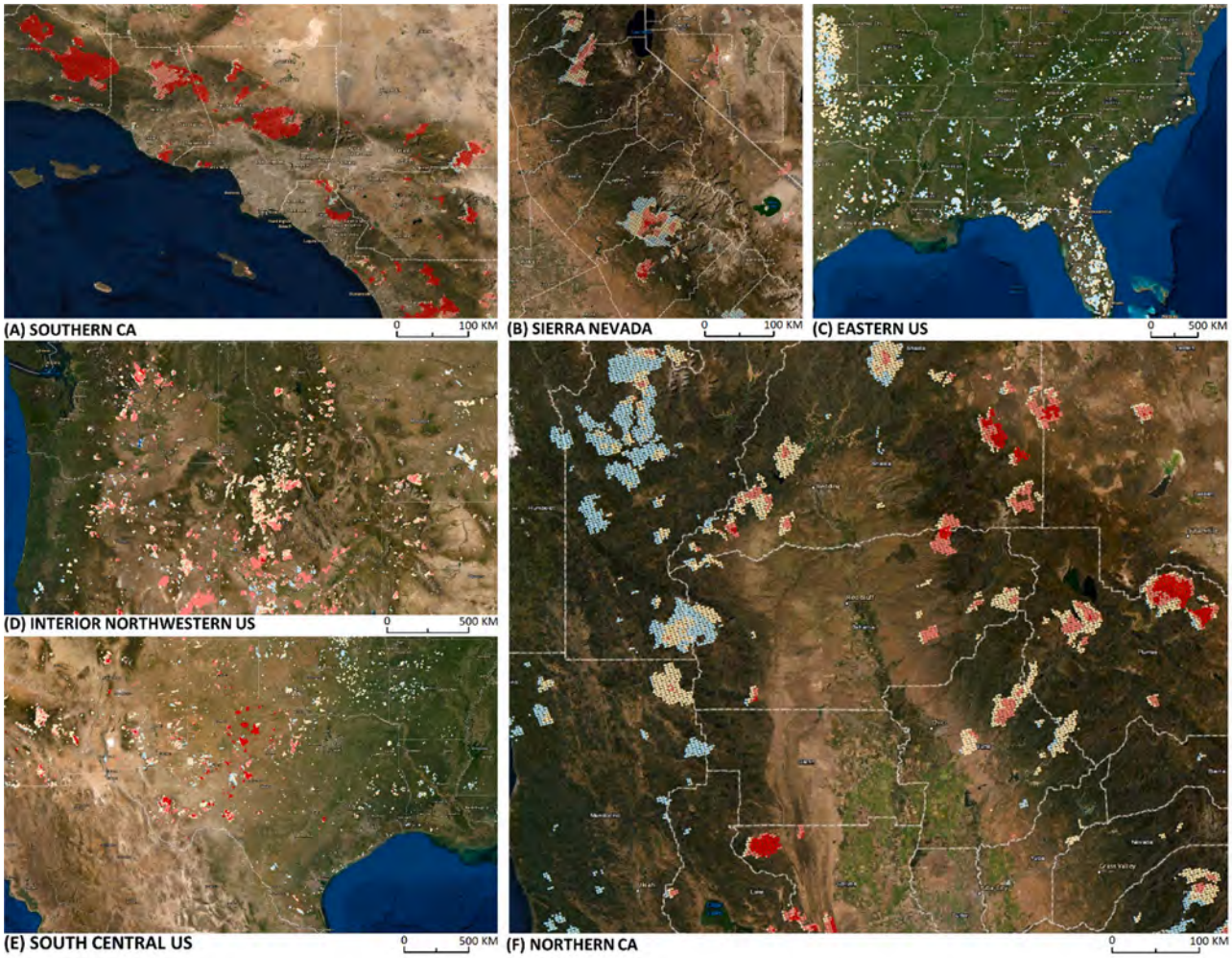

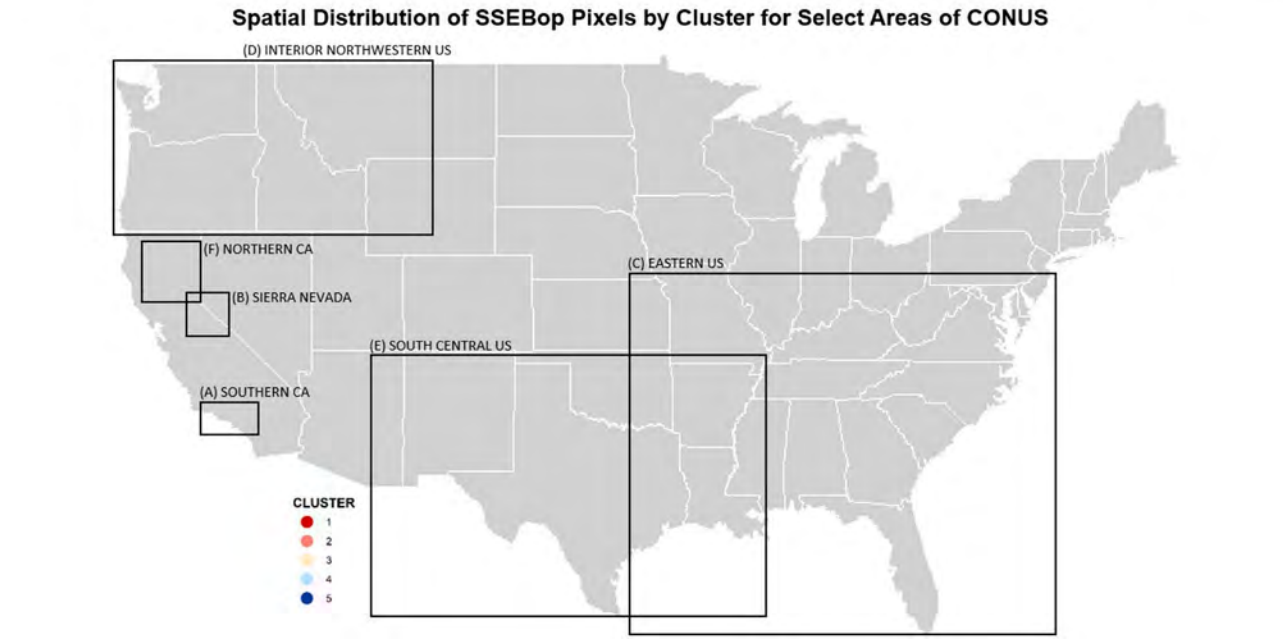

Fig. 8. Compilation of pixel cluster assignment for select areas around the US. Each colored dot represents the centroid of a SSEBop pixel and color designates pixel cluster assignment. Basemapping imagery from ArcMap v10.8. Service layer credits include "Esri, DigitalGlobe, GeoEye, Earthstart Geographics, CNES/Airbus DS, USDA, USGS, AeroGRID, IGN, and the GIS User Community.

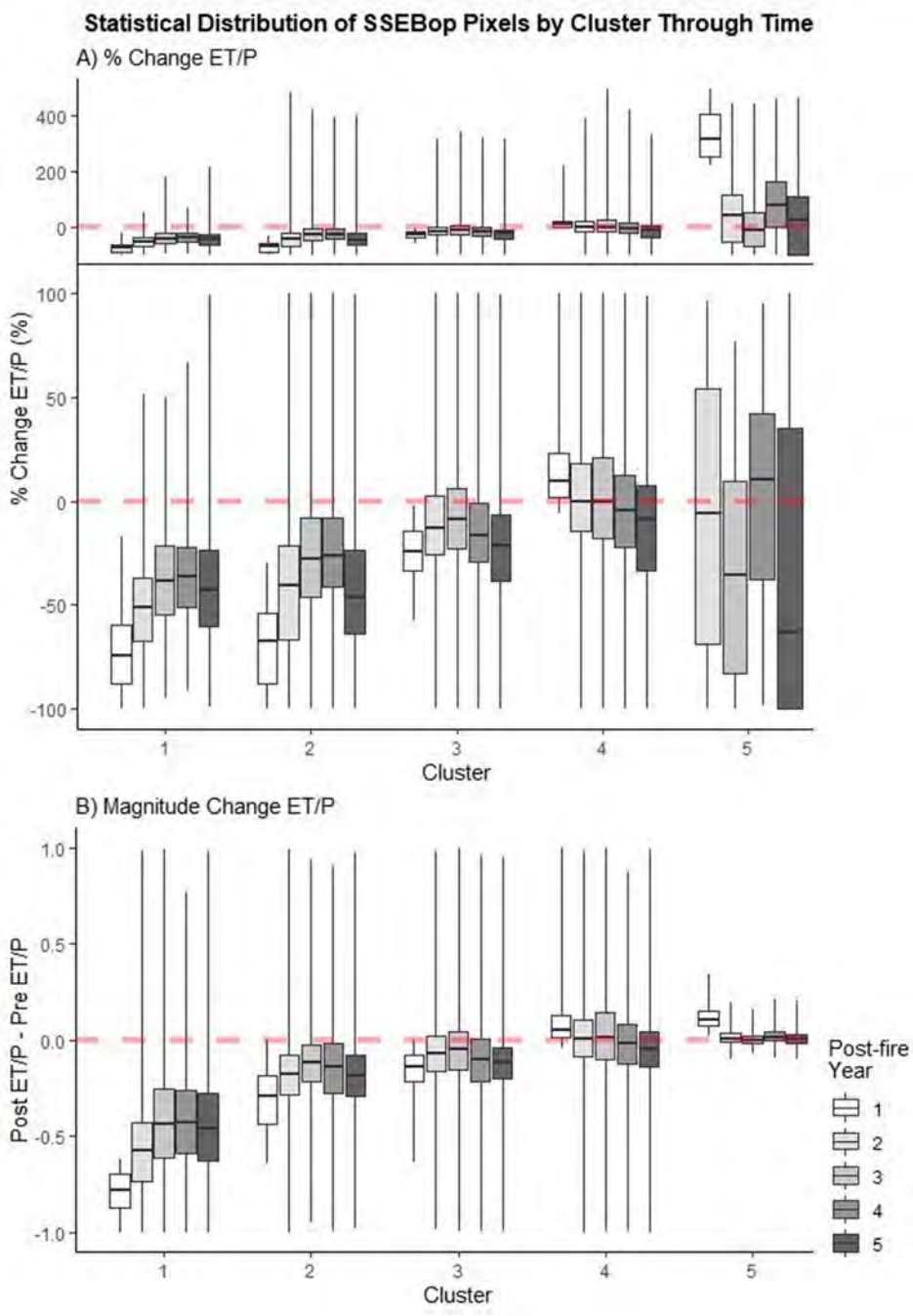

Fig. 9. Boxplots of ET/P response over time by cluster. (A) Percent change in ET/P by cluster through time, calculated as the percent change in post-fire ET/P years one through five from mean pre-fire ET/P. Plot provided at two different y-scales to show the large percentage increase in cluster 5 in post-fire year one (y-axis scale extended to 400% in top plot). (B) Magnitude change in ET/P by cluster, calculated as the change in post-fire ET/P years one through five from mean pre-fire ET/P. Zero change from pre-fire mean ET/P indicated by dashed, horizontal, red lines. Boxplot center bars indicate median, boxplot hinges are 25th and 75th percentiles, and whiskers are the largest value less than 1.5*IQR ± each hinge. (For interpretation of the references to color in this figure legend, the reader is referred to the web version of this article.)

(clusters 1 and 2), ET/P ratios are still only approximately 50% of their pre-fire values by post-fire year five. The R80P recovery metric substantiates this finding (Fig. 10A). By post-fire year five, the median ET/P of cluster 1 pixels remain below 80% of their pre-disturbance ratios. Cluster 2 pixels are at nearly 80%, and clusters 3, 4, and 5 have recovered back to, and in some cases exceeded, pre-fire ET/P.

The greater the initial departure from pre-fire ET/P, the steeper the recovery trajectory slope during the first five post-fire years (e.g., cluster 1 in Fig. 9A and B; cluster 1 in Fig. 10B). Boxplots of the YrYr recovery metric follow this trend: the greater the initial disturbance, the greater the magnitude of recovery towards pre-fire ET/P occurs at each annual time-step (Fig. 10B). Clusters with elevated ET/P in post-fire year one relative to the pre-fire condition (clusters 4 and 5) approach pre-fire ET/P through time from the opposite direction (Fig. 10B). Tukey HSD pairwise comparisons of ANOVA tests show that the R80P and YrYr recovery metrics significantly differ between all clusters ($p \leq 0.05$). In contrast, the RRI is not significantly different for any pairwise cluster comparison (data not shown).

3.2. Drivers of ET/P response

Many independent variables lack explanatory power at the CONUS scale. This is illustrated by the few significant correlations and low R^2 of CONUS-scale MLR models (Table 3) (e.g., "all pixels" scenario MLR $R^2 = 0.09$, "cluster 3" scenario MLR $R^2 = 0.12$) and is expected given the substantial overlap in independent variable distribution when data are subset by cluster only (not further into regions) (SM Figure B). The only overarching CONUS-scale trends identified are loose and include greater reductions in post-fire ET/P at more westerly longitudes ("all pixels" longitude R = 0.23, MLR coefficient = 0.27 (Table 3)) and with larger

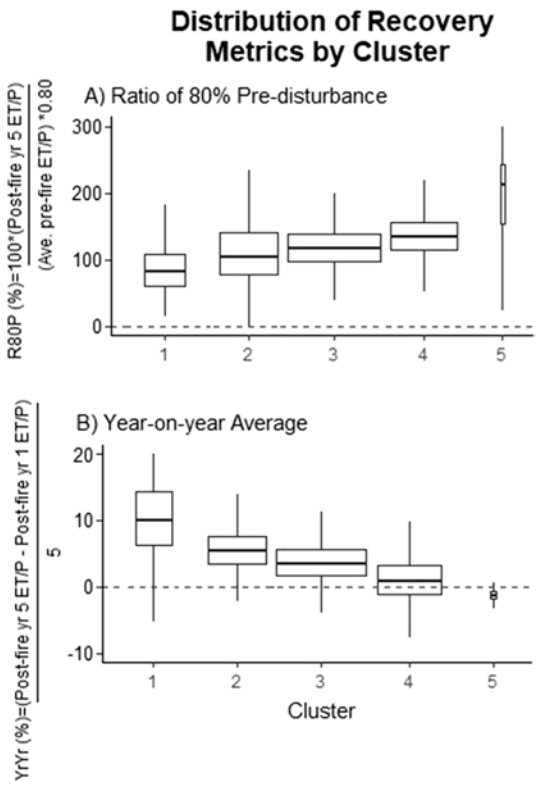

Fig. 10. Boxplots of Ratio of 80% Pre-disturbance and Year-on-year Average recovery metrics by cluster. (A) R80P recovery metric. Y-axis is the percentage recovered back to 80% of the pre-fire mean ET/P by post-fire year four or five (shown in y-axis label equation as five), whichever is greater, with 100% being exactly 80% of the pre-fire mean ET/P. (B) YrYr recovery metric. Y-axis is the average annual post-fire change in ET/P in the first five post-fire years, with negative values indicating an average loss in ET/P in each post-fire year one through five. Boxplot center bars indicate median, boxplot hinges are 25th and 75th percentiles, and whiskers are the largest value less than 1.5*IQR ± each hinge. Box widths indicate sample size. Per ANOVAs and Tukey HSD pairwise comparisons, all clusters are significantly different from all other clusters for the R80P and YrYr metrics; no cluster is significantly different from any other cluster for the RRI metric (not shown).

percentages of high burn severity area ("all pixels" high burn severity R = -0.30, MLR coefficient = -0.12).

MLR model performance is improved in many of the sub-CONUS-scale models (Table 3). Unique relationships emerge at smaller scales that are masked by contradictory relationships in CONUS-scale datasets. Variable relationships between ET/P response and pre-fire vegetation type provide good examples: in the Great Plains EPA ecoregion, more pre-fire shrub/scrub cover correlates with greater ET/P reduction (R = -0.32), while the opposite is true in the Southern Semi-arid Highlands (R = 0.23) (Table 3). More evergreen forest correlates with bigger ET/P reductions in the Southern Semi-arid Highlands (R = -0.26) and Northern Forests (R = -0.48), while the opposite is true in the Northwestern Forested Mountains (R = 0.23), Marine West Coast Forests (R = 0.33), and Tropical Wet Forests (R = 0.26). Grassland/herbaceous cover only exhibits control over ET/P response in the Great Plains (R = 0.28).

In some EPA ecoregions, we can better account for the high variability in the ET/P response by further subsetting ecoregions into cluster groups. For example, MLR R^2 increased from 0.12 to 0.58 when only cluster 3 pixels located in the Northern Forests EPA ecoregion were analyzed (SM Table C). No significant correlations are identified among cluster 2 or 3 pixels in Mediterranean California or cluster 4 pixels in the Great Plains and Southern Semi-arid Highlands ecoregions (SM Table C). More detailed studies are needed in these areas.

The direction of correlations between post-fire ET/P response and burn severity classification is consistent among the sub-CONUS-scale datasets. Where burn severity and ET/P response are significantly correlated (all pixels, cluster 1, cluster 3, every EPA ecoregion except North American Deserts and Tropical Wet Forests (Table 3)), low burn severity area is consistently associated with smaller ET/P reductions and high burn severity with larger reductions. Standardized MLR model coefficients show that burn severity is one of the most powerful explanatory variables for some datasets (Mediterranean California and Southern Semi-arid Highlands EPA ecoregions) (Table 3).

Prior work suggests that landscape response to burn severity depends on vegetation type (Lentile et al., 2007; Minnich, 1983). To test this, we select "pure" pixels (1 km pixel underlain by at least 75% of the same 30 m NLCD pre-fire vegetation type) of each of the CONUS's dominant fire-prone vegetation types (evergreen forest, shrub/scrub, grassland/herbaceous, emergent wetland) and break out by EPA ecoregion (Table 4). High burn severity is ubiquitously negatively correlated with more evergreen forest. However, there are no significant correlations between shrub/scrub cover and high burn severity in any of the EPA ecoregions. Among the grassland/ herbaceous pixels, correlation direction is inconsistent: high severity burns may promote increased post-fire ET/P in the Northern Forests and Great Plains (positively correlated) but reduced post-fire ET/P in the Temperate Sierras (negatively correlated). For most EPA ecoregions, although the biggest post-fire year one percent ET/P reductions often occur in shrub-scrub pixels, the magnitude change in ET_a is greatest in evergreen forest (Table 4).

3.2.1. *Burn scar scale assessment*

The explanatory power of independent variables at the burn scar scale is evaluated. The Zaca Fire (Fig. 5) occurred in the Mediterranean California EPA ecoregion (Table 3: Mediterranean California $R^2 = 0.12$) and the High Park (Fig. 6) and Rim fires (Fig. 7) in the Northwestern Forested Mountains EPA ecoregion (Table 3: Northwestern Forested Mountains $R^2 = 0.23$). MLR model performance is slightly improved when data are broken out by individual fire (Table 3: Zaca Fire $R^2 = 0.33$, High Park Fire $R^2 = 0.26$, Rim Fire $R^2 = 0.36$). The fact that SWE and ET/P response are not significantly correlated at the EPA ecoregion scale (Table 3) but are at the burn scar scale (Zaca Fire R = 0.25, High Park Fire R = -0.30, Rim Fire R = -0.20) is further evidence that some relationships are so site-specific, sub-regional scale analysis is required to identify them. Note that, despite significant correlations, the SWE variables' MLR coefficients are small or insignificant in all three MLR models.

Lithology accounts for a portion of the post-fire ET/P response variability at both the High Park (Table 3: percent unconsolidated MLR coefficient = 0.24) and Rim Fire areas (percent metamorphic MLR coefficient = 0.28). Pre-fire PDI (MLR coefficient = 0.21) and the amount of evergreen forest (MLR coefficient = 0.28) are drivers of post-fire ET/P response at the Zaca Fire. Interestingly, correlation direction between pre-fire vegetation types and post-fire ET/P response are opposite between the High Park Fire (percent evergreen forest R = -0.30, percent shrub/scrub R = 0.34) and the greater Northwestern Forested Mountains EPA ecoregion (percent evergreen forest R = 0.23, percent shrub/scrub R = -0.24). Neither variable is significant in the High Park Fire's MLR model. This indicates that even within the same EPA Level I ecoregion, some trends do not apply to all locations universally.

Burn severity is the most influential variable in the MLR models of all three fires (largest MLR coefficients) (Table 3). At the Zaca Fire, high burn severity correlates with annual average precipitation (R = 0.35), pre-fire shrub/scrub cover (R = -0.29), and pre-fire grassland/ herbaceous cover (R = -0.43). At the High Park Fire, high burn severity correlates with average annual precipitation (R = 0.44), average maximum annual temperature (R = -0.49), SWE (R = 0.59), AWC (R = 0.35), elevation (R = 0.57), pre-fire evergreen forest (R = 0.57), pre-fire shrub/scrub cover (R = -0.56), and pre-fire grassland/ herbaceous cover (R = -0.37). At the Rim Fire, high burn severity correlates with slope (R = -0.21), pre-fire evergreen cover (R = 0.23), and pre-fire shrub/scrub

Table 3

Pearson's R correlation and MLR standardized coefficients for each scenario (dataset) evaluated, including all pixels, clusters one through five, the three individual fires (High Park, Zaca, Rim), and EPA Level I ecoregions (bottom panel). R only provided when ≥ 0.20 ("–" indicates R < 0.20), and all R values shown are statistically significant ($p \leq 0.05$ using Spearman (three individual fires) or Pearson (all other scenario data subsets) method for significance). No models are built for the cluster 4 or North American Deserts EPA Level I ecoregion scenarios because there are no correlation coefficients ≥ 0.20 for either. Correlation coefficients are used to select variables for MLR models to determine variable importance; if collinear, the independent variable with the highest R value is selected for subsequent analysis to reduce overfitting (an underlined coefficient in the "Pear. Corr. Coeff." column indicates collinearity between independent variables (R ≥ 0.70) within that scenario data subset; "/" indicates that a variable is not included in the MLR model due to collinearity between that variable and at least one other variable in the scenario data subset). "*" indicates the MLR coefficient is insignificant. Cell color indicates the magnitude of the cell value. For example, ET/P response for pixels burned in the Zaca Fire is negatively correlated with high burn severity (R = -0.41) meaning that pixels with higher percentages of high burn severity areas have greater reductions in post-fire ET/P. The percent of high burn severity area is the most influential variable to ET/P response (MLR standardized coefficient = -0.52).

Pearson's R Correlation and Multiple Linear Regression Coefficients

		ALL PIXELS		CLUSTER 1		CLUSTER 2		CLUSTER 3		CLUSTER 5		HIGH PARK FIRE		ZACA FIRE		RIM FIRE	
		%ΔET/P		%ΔET/P		%ΔET/P		%ΔET/P		%ΔET/P		%ΔET/P		%ΔET/P		%ΔET/P	
	VARIABLE	Pear. Corr. Coeff.	MLR Coeff.	Pear. Corr. Coeff.	MLR Coeff.	Pear. Corr. Coeff.	MLR Coeff.	Pear. Corr. Coeff.	MLR Coeff.	Pear. Corr. Coeff.	MLR Coeff.	Pear. Corr. Coeff.	MLR Coeff.	Pear. Corr. Coeff.	MLR Coeff.	Pear. Corr. Coeff.	MLR Coeff.
Climate	Maximum daily temp. (deg C)	--		--		--		0.35	0.12	--		--		--		--	
	SWE (mm)	--		0.23	*	0.26	0.02	-0.24	*	-0.28	*	-0.30	*	0.25	0.06	-0.20	*
	PDI (-10 drought, 10 wet)	--		0.26	-0.04	-0.22	-0.05	--		0.25	*	--		0.22	0.21	--	
Geology/soils	AWC (cm water soil volume^{-1} km^{-1})	--		--		--		--		-0.23	/	--		--		--	
	% Metamorphic	--		--		--		--		--		--		--		0.28	0.30
	% Unconsolidated	--		0.21	*	--		--		--		0.26	0.24	--		--	
	% Sedimentary	--		-0.26	-0.10	--		0.20	0.07	--		--		--		--	
	% Igneous	--		0.20	/	--		-0.28	-0.04	-0.22	/	--		--		-0.22	/
Location	Latitude (DMS)	--		--		--		-0.31	/	0.34	*	/		/		/	
	Longitude (DMS)	0.23	0.27	0.42	0.52	0.30	0.46	0.31	0.18	-0.26	/	/		/		/	
Topography & solar irradiance	Elevation (m)	--		--		0.22	-0.15	-0.32	/	-0.36	-0.53	-0.28	/	--		--	
	Slope (%)	-0.23	0.08	-0.21	0.18	--		--		--		0.22	0.19	--		--	
	Solar radiation (MJ cm^{-2} yr^{-1})	--		--		--		--		--		--		--		--	
Pre-fire vegetation	% Deciduous	--		--		--		--		--		--		--		--	
	% Evergreen	--		0.24	0.34	0.42	0.45	--		--		-0.30	/	0.32	0.28	--	
	% Shrub/scrub	--		--		-0.28	/	--		--		0.34	*	--		--	
	% Grassland/herbaceous	--		--		--		--		--		--		--		--	
	% Emergent wetland	--		--		--		--		--		--		--		--	
Burn severity	% Low burn severity	0.28	/	0.23	0.07	--		--		--		0.32	/	0.41	/	0.52	0.52
	% Moderate burn severity	--		--		--		--		--		-0.20	*	0.22	-0.16	-0.36	/
	% High burn severity	-0.30	-0.12	-0.30	-0.26	--		-0.23	-0.07	--		-0.40	-0.25	-0.41	-0.52	-0.46	/
	Model R^2:		0.09		0.35		0.42		0.12		0.15		0.26		0.33		0.36
	Adjusted Model R^2:		0.09		0.35		0.42		0.12		0.13		0.25		0.33		0.36
	p-value:		<0.000		<0.000		<0.000		<0.000		<0.000		<0.000		<0.000		<0.000

		NORTHERN FORESTS		NORTHWESTERN FORESTED MOUNTAINS		MARINE WEST COAST FOREST		EASTERN TEMPERATE FORESTS		GREAT PLAINS		MEDITERRANEAN CALIFORNIA		SOUTHERN SEMI-ARID HIGHLANDS		TEMPERATE SIERRAS		TROPICAL WET FORESTS	
		%ΔET/P		%ΔET/P		%ΔET/P		%ΔET/P		%ΔET/P		%ΔET/P		%ΔET/P		%ΔET/P		%ΔET/P	
	VARIABLE	Pear. Corr. Coeff	MLR Coeff.	Pear. Corr. Coeff	MLR Coeff.	Pear. Corr. Coeff	MLR Coeff.	Pear. Corr. Coeff	MLR Coeff.	Pear. Corr. Coeff	MLR Coeff.	Pear. Corr. Coeff	MLR Coeff.	Pear. Corr. Coeff	MLR Coeff.	Pear. Corr. Coeff	MLR Coeff.	Pear. Corr. Coeff	MLR Coeff.
Climate	Maximum daily temp. (deg C)	0.37	/	0.22	0.19	--		--		-0.22	-0.07	--		--		--		0.26	0.07
	SWE (mm)	-0.69	-0.44	--		--		--		--		--		--		--		--	
	PDI (-10 drought, 10 wet)	0.53	0.10	--		0.33	0.46	0.43	0.58	--		0.22	0.13	--		0.25	0.21		
Geology/soils	AWC (cm water soil volume^{-1} km^{-1})	-0.38	/	--		--		--		0.29	0.18	--		0.23	0.16	0.24	0.22	-0.22	0.09
	% Metamorphic	0.50	/	--		--		--		--		--		--		--		--	
	% Unconsolidated	--		--		--		--		--		--		--		--		--	
	% Sedimentary	0.25	/	--		0.29	0.15	--		--		--		--		--		--	
	% Igneous	-0.60	-0.20	--		-0.28	-0.12	--		--		--		--		--		--	
Location	Latitude (DMS)	--		--		--		--		--		0.22	0.18	--		--		-0.28	-0.37
	Longitude (DMS)	--		--		-0.59	-0.63	--		--		--		-0.33	-0.20	--		-0.26	/
Topography & solar irradiance	Elevation (m)	-0.41	/	--		-0.31	-0.29	--		--		--		--		--		--	
	Slope (%)	-0.31	*	0.23	0.15	--		--		--		--		--		--		--	
	Solar radiation (MJ cm^{-2} yr^{-1})	-0.25	-0.09	--		--		-0.21	-0.14	--		--		--		--		0.21	/
Pre-fire vegetation	% Deciduous	--		--		--		--		--		--		--		--		--	
	% Evergreen	-0.48	-0.23	0.23	0.32	0.33	*	--		--		--		-0.26	-0.08	--		0.26	0.26
	% Shrub/scrub	--		-0.21	/	--		--		-0.32	-0.22	--		0.23	/	--		--	
	% Grassland/herbaceous	--		--		--		--		0.28	/	--		--		--		--	
	% Emergent wetland	--		--		--		--		--		--		--		--		0.24	0.17
Burn severity	% Low burn severity	0.51	0.11	0.26	0.31	0.32	/	0.24	0.11	--		--		0.57	/	0.23	0.20	--	
	% Moderate burn severity	--		--		-0.20	/	--		-0.20	-0.14	--		-0.38	-0.31	-0.20	/	--	
	% High burn severity	-0.48	/	-0.21	/	-0.43	-0.05	-0.23	-0.11	--		-0.26	-0.21	-0.26	/	-0.20	/	--	
	Model R^2:		0.67		0.23		0.71		0.25		0.17		0.12		0.24		0.15		0.23
	Adjusted Model R^2:		0.67		0.23		0.70		0.25		0.17		0.12		0.24		0.15		0.23
	p-value:		<0.000		<0.000		<0.000		<0.000		<0.000		<0.000		<0.000		<0.000		<0.000

Table 4

ET_a and ET/P response and recovery summarized by EPA Level I Ecoregion and pre-fire vegetation type. Pixels filtered so that only pixels at least 75% burned and comprised by at least 75% of the same pre-fire vegetation type are included; '—' indicates no pixels meet both filtering criteria for the combination or, for pixels that do meet both filtering criteria, not enough are mapped as high burn severity to evaluate Pearson's R correlation. Evergreen forest pixels: n = 30,711; shrub/scrub pixels: n = 42,802; grassland/herbaceous pixels: n = 12,268; emergent wetland pixels: n = 953. Mean pre-fire ET_a and ET/P are the averages for the five pre-fire years. For the percent and magnitude change in ET_a and ET/P columns and the YrYr column, redder hues indicate a reduction and bluer hues indicate an increase in the summary statistic relative to pre-fire average values. YrYr is the average annual magnitude change in ET/P in the first five post-fire years (equation provided in section 2.3). Pearson's R correlation is calculated for the percent of a pixel burned at high severity against post-fire year one ET/P percent change. All correlation coefficients are statistically significant ($p \leq 0.05$) using the Pearson method for significance.

		Pre-fire ET_a (mm) (mean)				**Pre-fire ET/P** (fraction) (mean)				**% Change ET_a** (%) (mean) post-fire year 1				**Magnitude Change ET_a** (mm) (mean), post-fire year 1				**% Change ET/P** (%) (mean) post-fire year 1				**Magnitude Change ET/P** (mm) (mean) post-fire year 1				**YrYr Recovery Metric** (fraction) (mean)				**Pearson's R Correlation** high burn severity *against* % change ET/P in post-fire year 1			
EPA Level I Ecoregion		EVERGREEN FOREST	SHRUB/SCRUB	GRASSLAND/HERBACEOUS	EMERGENT WETLAND	EVERGREEN FOREST	SHRUB/SCRUB	GRASSLAND/HERBACEOUS	EMERGENT WETLAND	EVERGREEN FOREST	SHRUB/SCRUB	GRASSLAND/HERBACEOUS	EMERGENT WETLAND	EVERGREEN FOREST	SHRUB/SCRUB	GRASSLAND/HERBACEOUS	EMERGENT WETLAND	EVERGREEN FOREST	SHRUB/SCRUB	GRASSLAND/HERBACEOUS	EMERGENT WETLAND	EVERGREEN FOREST	SHRUB/SCRUB	GRASSLAND/HERBACEOUS	EMERGENT WETLAND	EVERGREEN FOREST	SHRUB/SCRUB	GRASSLAND/HERBACEOUS	EMERGENT WETLAND	EVERGREEN FOREST	SHRUB/SCRUB	GRASSLAND/HERBACEOUS	EMERGENT WETLAND
5	Northern Forests	517	313	393	498	0.69	0.39	0.63	0.83	-28	23	1	-15	-140	72	2	-72	-38	13	-31	5	-0.26	0.05	-0.22	0.04	0.03	0.00	0.04	0.01	-0.68	--	0.48	<0.20
6	NW Forested Mountains	563	222	136	433	0.64	0.39	0.30	0.76	-34	-51	-52	13	-183	-107	-58	51	-29	-48	-46	17	-0.18	-0.18	-0.11	0.12	0.02	0.04	0.03	0.03	-0.44	<0.20	<0.20	<0.20
7	Marine West Coast Forests	883	569	--	--	0.65	0.30	--	--	-11	-18	--	--	-88	-97	--	--	13	-1	--	--	0.10	0.00	--	--	0.01	0.00	--	--	-0.25	<0.20	--	--
8	Eastern Temp. Forests	1210	1018	822	1066	0.96	0.79	0.63	0.88	-3	-3	-6	-1	-30	-34	-64	-7	2	1	-1	0	0.00	0.00	-0.04	0.00	-0.01	0.00	0.00	0.03	-0.44	<0.20	<0.20	-0.36
9	Great Plains	443	564	489	859	0.85	1.06	0.74	0.83	-23	-50	-13	-1	-116	-307	-69	-14	-30	-35	-13	12	-0.27	-0.41	-0.10	0.09	0.04	0.07	0.05	0.04	-0.29	<0.20	0.24	-0.29
10	North American Deserts	367	147	64	196	0.94	0.39	0.20	0.78	-48	-56	-52	-20	-165	-78	-38	-39	-41	-50	-45	-2	-0.36	-0.19	-0.10	0.02	0.07	0.05	0.05	0.15	<0.20	<0.20	<0.20	--
11	Mediterranean California	639	410	215	--	0.99	1.10	0.60	--	-64	-75	-65	--	-398	-302	-132	--	-60	-73	-59	--	-0.59	-0.78	-0.34	--	0.09	0.11	0.11	--	-0.45	<0.20	<0.20	--
12	Southern Semi-arid Highlands	577	354	199	--	1.06	0.90	0.64	--	-44	-21	-9	--	-257	-83	-18	--	-39	-25	-29	--	-0.42	-0.22	-0.19	--	0.08	0.05	0.04	--	-0.26	<0.20	--	--
13	Temperate Sierras	569	414	302	--	1.07	0.97	0.50	--	-27	-37	-50	--	-159	-174	-157	--	-26	-21	-42	--	-0.29	-0.23	-0.23	--	0.03	0.01	0.01	--	-0.21	--	-0.47	<0.20
15	Tropical Wet Forests	--	--	--	1258	--	--	--	1.02	--	--	--	2	--	--	--	21	--	--	--	-9	--	--	--	-0.10	--	--	--	0.03	-0.44	<0.20	<0.20	<0.20

cover (R = -0.21). These correlations are performed separately to illustrate the interconnectedness of variables and are not provided in the current publication; full correlation matrices are available upon request. Although many of the variables correlated with burn severity are not also significantly correlated with post-fire ET/P response, it may be possible to forecast post-fire ET/P in unburned areas given the consistent relationship between burn severity and post-fire ET/P response: burn severity could be predicted from the correlated landscape attributes and post-fire ET/P response inferred from the burn severity prediction.

3.3. *Attribution of ET/P shift to fire*

In post-fire year one, the majority of cluster 1, 2, and 5 pixels exhibit ET/P shifts outside one standard deviation of pre-fire ET/P (Fig. 2D). Conversely, ET/P changes in approximately half of cluster 3 pixels and most cluster 4 pixels are within one standard deviation, or the historical observed ET/P range. This suggests that the ET/P reductions observed in clusters 1, 2, and 5 are more likely a result of fire disturbance and less likely a result of natural, interannual ET/P variability.

DID regressions are used to further evaluate the role of fire in post-fire ET/P shifts on pairs of burned and unburned pixels from six different locations in the western US. Results from all 60 pairs (ten pairs of pixels per fire) are provided in SM Table D. Results from one randomly selected pair of pixels from each fire are plotted in Fig. 11. The regression coefficients for the DID variable are negatively correlated with annual ET/P in every pixel pair and are statistically significant ($p \leq 0.10$) for at least one pixel pair from each fire. However, DID coefficients for numerous pixel pairs from the PK Complex and Zaca Fire are not significant (SM Table D). Probability density functions (PDFs) of the percent difference in pre and post-fire annual ET/P for the same pixel pairs plotted in Fig. 11 show that post-fire ET/P differences increased substantially relative to pre-fire differences. In the post-fire period, ET/Ps of the unburned pixels are consistently higher than ET/Ps of their burned counterparts (Fig. 12).

At each burned pixel, Pettitt's test identifies a change in ET/P at the year preceding the fire (data distributions changed starting at post-fire year one) (Fig. 11, SM Table D). Possibly owing to the short length of the datasets and high annual ET/P variability, results for Pettitt's test are only significant for pixels in three of the six fires (LaBrea, Moonlight, Zaca). Pettitt's test also identifies significant shifts in pre-fire year one ET/P data for unburned pixels adjacent to the PK Complex and Zaca Fire areas.

Overall, results support the hypothesis that fires are a primary driver of post-fire ET/P shifts. Results from the PK Complex are the least definitive: although ET/P is initially reduced in burned pixels relative to unburned pixels, ET/P recovered quickly and closely matched the unburned pixels' behavior after post-fire year one (Fig. 11; behavior is similar for the other nine pairs). The PK Complex's ten burned pixels are in areas mapped at low to moderate burn severity and were comprised of varying fractional areas of evergreen forest and grassland/ herbaceous cover before the fire. Vegetation recovery may have been rapid in the low burn severity areas and the grasslands. Results from the Zaca fire pixel pairs were also irresolute. Given its large percentage of high severity burn area and big post-fire year one ET/P reductions (Fig. 5), the lack of significant DID regression coefficients at the Zaca Fire is unexpected.

4. Discussion

4.1. *Spatial and temporal ET/P response*

This is the first study to evaluate wildfire-induced ET_a and ET/P modification at the CONUS extent. We identify locations where the direction and magnitude of post-fire ET/P shifts may be more easily inferred (regions with low inter and intra-fire response variability) and less easily inferred (high inter and/or intra-fire response variability). Where variability is high, predicting the potential hydrologic response of an unburned area to fire may be difficult.

Our data indicate high intra-fire ET/P response variability at the Rim Fire burn area (western slope of Sierra Nevada) (Fig. 7). It is notable that the fire's burn severity patterns were also variable (middle panel of Fig. 7) and that the current study and previous work (Blount et al., 2020) link post-fire ET_a response to burn severity. Insets of other burned areas in Northern California (Fig. 8F) and the Sierra Nevada specifically (Fig. 8B) show qualitatively that other burns in the fire's vicinity have also had variable intra-fire ET/P response (pixels assigned to clusters 1,

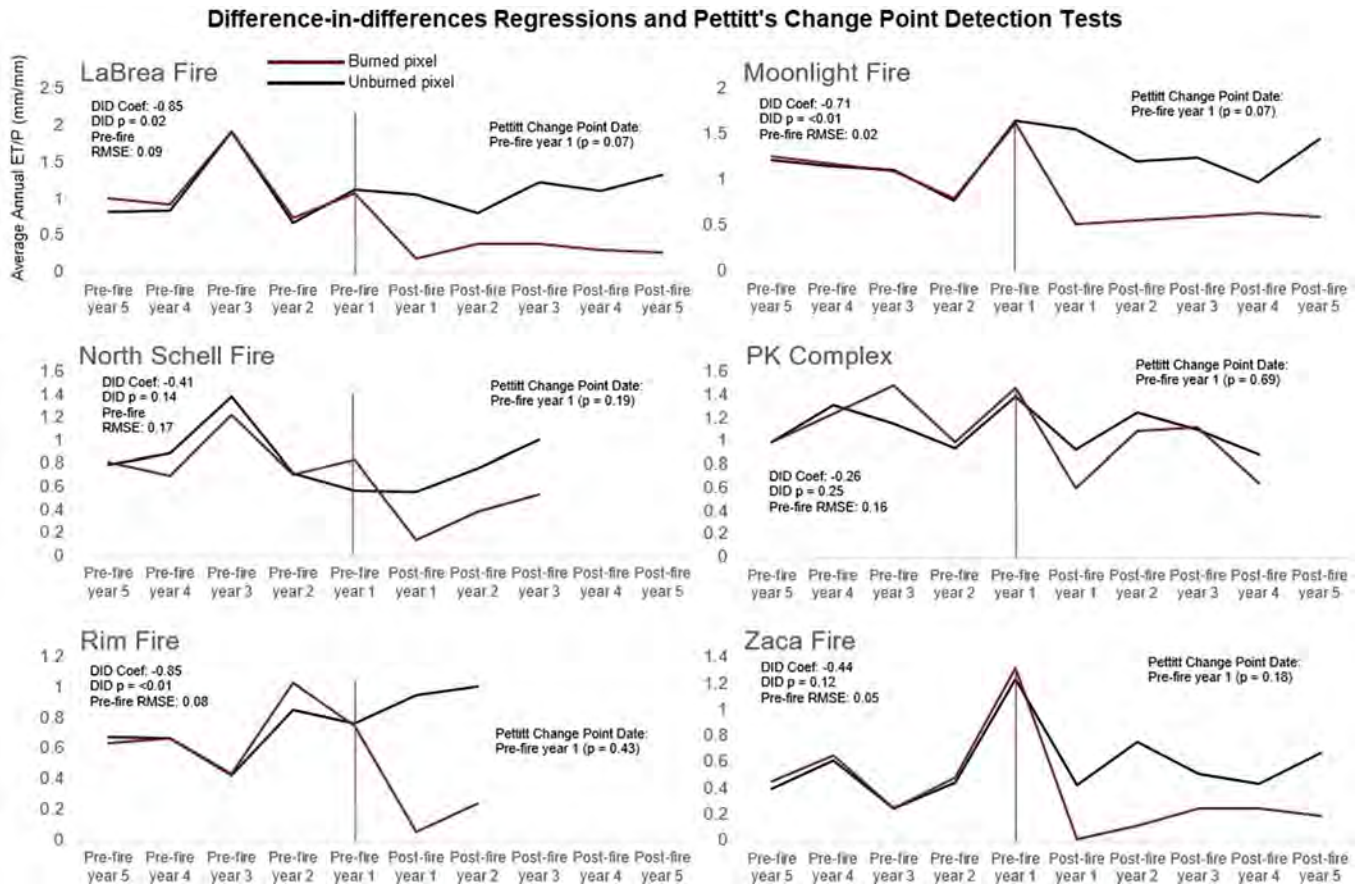

Fig. 11. Difference-in-difference (DID) regression and Pettitt's change point detection test results for paired burned and unburned pixels from select fires throughout the western CONUS. One fire from each of the EPA Level I Ecoregions that contain the majority of cluster 1 pixels was randomly selected (Great Plains: PK Complex Fire [TX3289209866620110413]; Mediterranean California: LaBrea Fire [CA34936120027200908]; Northwestern Forested Mountains: Moonlight Fire [CA40220120736200709 03]; North American Deserts: North Schell Fire [NV3967911463320120612]). Pixels from the three case study fires with pixels assigned to cluster 1 are also analyzed (Rim Fire [CA3785712008620130817]; Zaca Fire [CA34695119659200707 04]). Ten pairs of burned and unburned pixels are selected for each fire; results from only one randomly selected pair from each fire are plotted in the figure. Unburned pixels are selected from areas adjacent to and outside of fire perimeters. Burned pixels belong to cluster 1 and are selected for having the most similar pre-fire ET/P behavior to the paired, unburned pixel according to the root mean squared error (RMSE) of each pixels' annual pre-fire ET/P for the five years preceding the burn event. 'DID Coef' is the value of the DID coefficient variable, 'DID p' is the p-value of the DID coefficient. As detected by Pettitt's change point detection tests, dates of major, behavioral shifts in the burned pixels' average annual ET/Ps are indicated with red vertical bars. (For interpretation of the references to color in this figure legend, the reader is referred to the web version of this article.)

2, 3, and 4). This contrasts with areas where inter and intra-fire response variabilities are low, such as in southern California or the eastern US (Fig. 8A and C, respectively). Work conducted by Lydersen et al. (2014) identified several landscape attributes that correlated with burn severity class at the Rim Fire (e.g., elevation, vegetation composition), many of which had steep gradients in the burned area. This may explain the patchy burn severity patterns (Lydersen et al., 2014) (see also Goulden and Bales (2014)). Lydersen et al. (2014) also noted that highly unstable weather conditions occurred shortly after ignition and likely contributed to the fire's dynamic behavior and resultant patchy burn severity. Thus, because the area is ecologically, topographically, and climatically diverse, and based on evidence from surrounding areas, it may have been foreseeable that a fire on the western slope of the Sierra Nevada would result in variable burn severity patterns and consequently, variable ET/P response. The current work identifies statistical relationships between burn severity and various landscape attributes (corroborated by prior research (Lentile et al., 2007; Stevens-Rumann et al., 2016)), suggesting that it may be possible to predict post-fire ET/P response from a burn severity prediction.

Analysis of cluster assignment and incident type suggests that wildfire tends to reduce ET/P more than prescribed fire. Prescribed fires are also more commonly associated with lower burn severity than are wildfires. These results agree with previous findings that prescribed burns often correspond with lower burn severities, smaller fire sizes, and are less likely to increase post-fire average annual discharge (Hallema et al., 2018). Numerous studies summarized by Goeking and Tarboton (2020) also show that non-stand-replacing drought, beetle kill, and fire disturbance can increase ET_a. This further corroborates our work and may be relevant to land managers prescribing fire to reduce fuel load. Where ET_a increases within a year of prescribed burn treatment (i.e., cluster 4 pixels), vegetation may be regrowing rapidly and repeated treatment may be required to maintain low fuel stock (Elliot et al., 2010). In areas managed for water supply, the effect of prescribed burns on water yield might also be considered (an actively debated, nuanced topic that seems to be highly site-specific (Bart et al., 2021)). Relative to pixels in clusters 1 and 2, a larger percentage of cluster 3 and 4 pixels are characterized by post-fire year one ET/P ratios within one standard deviation of their pre-fire average ET/P (Fig. 2D). In other words, prescribed burns are more likely to cause ET/P shifts within the range of background variability than wildfires.

There is a pattern in numerous burned areas where pixels with smaller post-fire ET/P modifications are located at the burn perimeter and greater ET/P reductions are located in the interior (e.g., Rim Fire (Fig. 7); additional burned areas shown in Fig. 8F). This may occur because fires naturally burn out or are successfully extinguished where conditions promote milder fire behavior, such as where there is a shift in

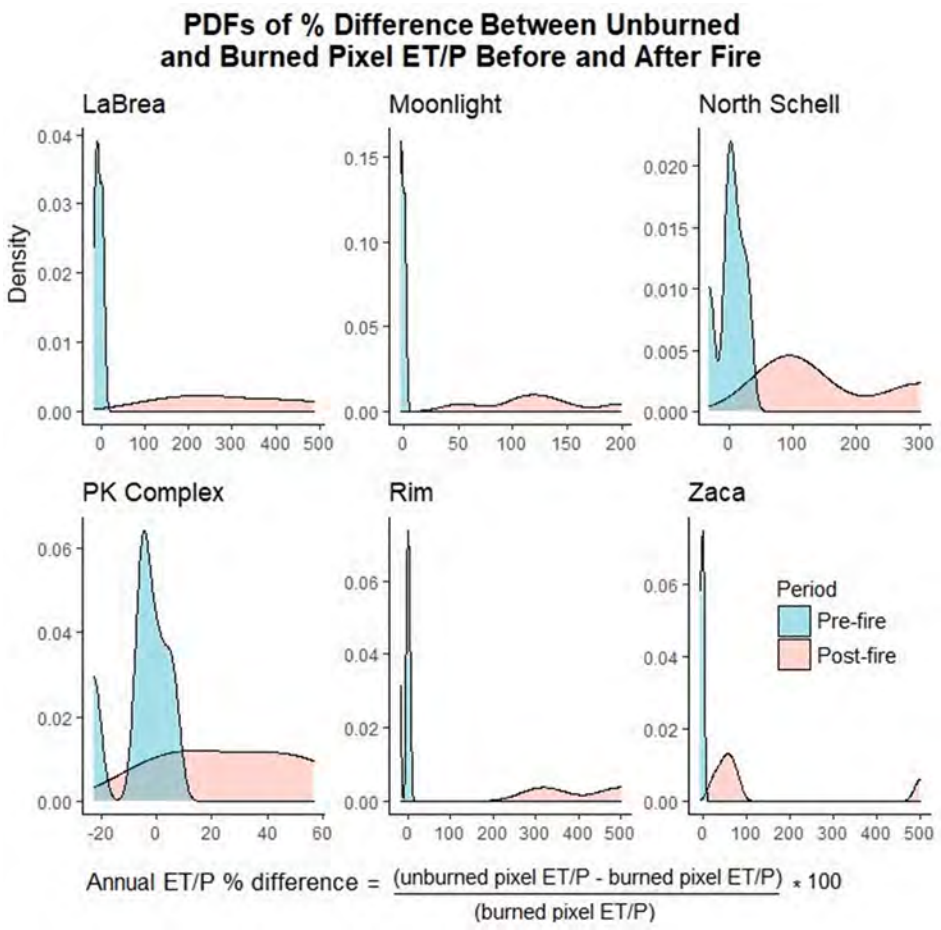

Fig. 12. Probability Density Functions (PDFs) of the percent difference between unburned and burned pixel ET/P before and after fires for the same six pixel pairs shown in Fig. 11 (one pair of pixels per fire). X-axis provides the percent difference of each unburned-burned pixel pair's annual ET/P for the five years preceding the fire (blue) and the two to five years following the fire (red) (two post-fire years of data for Rim Fire, three for North Schell Fire, four for PK Complex fires, five for the remaining). Negative values indicate that for a given year, the burned pixel's ET/P is greater than the unburned pixel's ET/P (rendering a negative percent change). For Rim and Zaca fires, percent difference in post-fire year one ET/Ps are 1,575% and 2,140%, respectively; reduced to 500% for plotting purposes. (For interpretation of the references to color in this figure legend, the reader is referred to the web version of this article.)

the density and/or condition of the fuel inventory (e.g., where natural or artificial fire breaks are located) or where topography and/or weather patterns promote lower intensity burning conditions (Calkin et al., 2014; Hansen, 2018; USDA Forest Service, 2003; Whitman et al., 2018). Furthermore, at the perimeter, fire may be less likely to fully consume vegetation and plant recovery rates may be faster due to greater abundance of onsite and proximity to off-site seed sources (Lentile et al., 2007; Minnich, 1983). The pattern may be further evidence that where land management promotes milder fire behavior and smaller patches of high burn severity area, the risk of post-fire water budget modification may be diminished.

4.2. *Relationships between ET/P response and landscape attributes*

We establish that the influence of certain landscape attributes on post-fire ET/P response is not uniform across the CONUS, such as pre-fire vegetation type (Table 3, SM Table B). As such, only results from our sub-CONUS-scale models can be used to meaningfully inform the potential ET_a or ET/P response of a particular location or landscape condition to fire and provides a basis for further work at finer spatial scales. Some regions of the CONUS are so diverse that ET/P response did not correlate with any variables, even when broken out by both cluster assignment and EPA ecoregion. Elsewhere, breaking out EPA regions by cluster increased explanatory power (all pixels in the Great Plains: $R^2 = 0.17$, only cluster 1 pixels in the Great Plains: $R^2 = 0.45$).

The relatively small R^2 of even our burn scar scale MLR models suggests that relationships between post-fire ET/P response and certain landscape attributes may be non-linear, or that one or more potentially relevant independent variables have been omitted. We do not include myriad static and dynamic variables previously shown to influence post-fire watershed hydrology. Pre-fire vegetation management tactics are not represented in the NLCD land cover dataset (e.g., thinning, ladder fuel removal) (Hankins, n.d.; Lake et al., 2017; Roche et al., 2018) nor are explicit measures of vegetation density (Pyne, 2016, 2012, 2011; van Wagtendonk et al., 2018). Time since last burned (Lydersen et al., 2014), post-fire climatic conditions (save annual precipitation in evaporation ratios) (Frazier et al., 2018; Roche et al., 2020, 2018), insect infestation (Vanderhoof and Williams, 2015), and long-term vegetation conversion (Keeley and Keeley, 1984; Landesmann et al., 2021; Rodman et al., 2020; Rother and Veblen, 2016) are also not accounted for. These, and the potential for ML approaches to tease out non-linear relationships, could be considered in future work.

We *do* establish spatially and directionally consistent relationships between ET/P response and burn severity classification. We also identify patterns between burn severity, ET/P response, and pre-fire vegetation type (Table 4) and show that the magnitude change in post-fire ET/P is often greatest in evergreen forest. This is sensical as pre-fire ET_a and ET/P are also highest in the evergreen forest pixels in the majority of EPA ecoregions, and because it is well-established that forests have higher ET_a rates than other vegetation types (Zhang et al., 2001). We also show that the rate of ET/P recovery is inconsistent across vegetation types and regions (Table 4). Per the YrYr recovery metric, ET/P recovery in emergent wetland is twice as fast as recovery in evergreen forest and three times as fast as in shrub/scrub and grassland in the North American Deserts EPA ecoregion. In the Great Plains, ET/P recovery is fastest in shrub/scrub ecosystems. In the Southern Semi-arid Highlands, recovery is fastest in evergreen forest. This has important management implications and may help land managers set appropriate expectations about the potential duration of fire-induced hydromodification.

Past work shows that, in some locations, forested areas exposed to

high burn severity are more likely to convert to a different type of cover (i.e., grassland or shrub/scrub) than other vegetation types (Barton and Poulos, 2018). This will likely affect energy budgets, and therefore post-fire ET_a, as evergreen forests have lower albedos than their deciduous, shrubby, and herbaceous alternatives ((Jin et al., 2012; van Wagtendonk et al., 2018)). Burn severity may also impact post-fire soil moisture and therefore watershed recovery. In their modeling study, Atchley et al. (2018) observed reduced ET_a in both low and high burn severity areas, which should have increased soil moisture. However, in the high burn severity areas only, the increases elicited by the ET_a response were eclipsed by larger magnitude reductions in infiltration which increased the runoff response. The high burn severity areas had comparatively drier soils as a result. It has also been shown that post-fire ET_a modification is linked to the geology that controls subsurface water availability (Maina and Siirila-Woodburn, 2020). The current study also identifies loose relationships between geologically-driven AWC and ET/P response at the EPA ecoregion scale and lithology at multiple scales (Table 3, SM Tables B and C). Land management decisions may account for these nuances by considering which can be managed (e.g., actively treating fuel loads to reduce the risk of high burn severity) and which cannot (e.g., lithology).

4.3. Limitations

Correlations between solar radiation, slope, and ET/P response are low (Table 3) despite literature indicating that higher burn severities tend to occur in drier and warmer landscape positions (often aspect driven) (Alexander et al., 2006; Bigler et al., 2005; Pereira et al., 2016) and our finding that burn severity and ET/P response are related. Summaries of our data support the literature: in north-facing cluster 1 pixels (aspects between 350 and 10 degrees), the mean percent change in post-fire year one ET/P is −77%, versus −97% in entirely south-facing cluster 1 pixels (aspects between 170 and 190 degrees). The SSEBop product's moderate spatial resolution may mute the sub-grid heterogeneity in the native slope and aspect 30 m data and mask the significance of these relationships with post-fire ET/P response (Dillon et al., 2011). Similarly, quantifying solar irradiance at the annual timestep may mute any explanatory power of the seasonal energy balance (Buffo et al., 1972; Sellers, 1965). Aggregating to the annum also reduces insight into the shape of the ET/P response.

While the moderate spatial and temporal resolution of the input data limits our ability to detect smaller-scale effects of topography, climate, and land surface cover, the computational requirements of a CONUS-scale analysis using higher resolution data would be prohibitive. The 1 km SSEBop product is a well-established dataset with numerous use-cases in the literature and well-documented validations (Chen et al., 2016; Savoca et al., 2013; Senkondo et al., 2019; Singh and Senay, 2015; Tobin and Bennett, 2019). The 30 m Landsat-based model is not yet established as a primary data product and is still being developed and revised (Senay, 2018; USGS EROS Customer Services, n.d.). The coarser-resolution 1 km product is also less likely to contain error-prone outliers because values are averaged over a larger spatial extent.

The current study uses burn severity mapping generated from dNBR. We acknowledge that the ability of satellite-derived metrics to accurately capture soil burn severity has been questioned (Keeley, 2009; Kolden et al., 2015). Satellite-derived measurements aggregate fire effects at the spatial grain of the sensor which can introduce uncertainty and smooth out underlying heterogeneity. And, because NBR is based on spectral properties of ground or above-ground cover, it does not sample the subsurface and therefore misses aspects of fire-induced soil modification (Cansler and McKenzie, 2012; Key and Benson, 2006). While our use of MTBS burn severity data may increase result uncertainty, dNBR and Relative differenced NBR (RdNBR) are widely used indices for assessing burn severity (Cansler and McKenzie, 2012). Furthermore, field-verified burn severity assessments that include subsurface observations are not currently available at the CONUS scale.

4.4. Effect of fire versus background climate variability

Due to the overarching influence of climate on hydrologic processes, establishing cause-and-effect relationships between suspected forcings and shifts in hydrologic data can be challenging (Beyene et al., 2021; Goulden and Bales, 2014; Hallema et al., 2018). It has been shown that in some parts of the CONUS, post-fire streamflow may be primarily controlled by interannual climate variability and only secondarily by the landscape modifications conferred by fire (Hallema et al., 2018). Inferring causality from statistical correlations alone can be misleading due to feedbacks and data limitations (Müller and Levy, 2019).

Analysis of burned and unburned pixel pairs indicates fire disturbance played a role in post-fire ET/P reductions (Fig. 11). However, results from two of the six fires tested are insignificant. High variability in the ET_a data, the short temporal length of the datasets, and post-fire vegetation recovery could be reducing the signal detection capabilities of the statistical tests applied. Alternatively, overarching climate patterns may be strong enough to overwhelm any fire-induced signals. At the 2011 PK Complex fire in Texas, cumulative precipitation during the water year the fire occurred was low relative to the long-term average. Drought conditions wrought by a La Niña in the southern US in 2011 (Fernando et al., 2016) were a likely driver of the widespread fire activity in Texas that year (DeBano et al., 1998; van Wagtendonk et al., 2018). But evaporation ratios were reduced both inside and outside the PK Complex's burn perimeter during post-fire year one (Fig. 11). Regional rainfall was above average in 2012 and may have contributed to smaller ET/P ratios in burned and unburned areas alike. Although reductions were larger in the burned PK Complex pixels, the strong, super-imposed climate signal may have muted the significance of those reductions.

5. Conclusions

This is the first study to evaluate post-fire ET_a response at the CONUS extent. Results can help inform land managers of potential post-fire water budget shifts and provide the basis for future work at finer spatial scales. ET/P is reduced in 82% of pixels during post-fire year one, the largest occurring in the arid southwest. Moderate reductions also occur throughout western states, and small to negligible decreases occur throughout the CONUS, especially in the eastern US. Eighteen percent of pixels observe negligible to moderate ET/P increases, including numerous pixels in the eastern CONUS, around burn perimeters in the mid to lower western states, within prescribed fires, and in wet regions west of the 100th meridian (the longitudinal line at 100 degrees west of the prime meridian). Five years after fires, evaporation ratios recover to only approximately 50% of their pre-fire value in pixels with the largest initial reductions (pixels assigned to cluster 1). A comparison of burned and unburned pixel pairs indicates fire is the primary driver of the shifts, but also that there is high background interannual variability in the ET_a and precipitation data.

Owing to its high topographic, climatologic, and ecologic variability, the influence of some landscape attributes on the post-fire ET/P response is not uniform across the entire CONUS (e.g., pre-fire vegetation type). If interested in the vulnerability of a particular location or landscape condition to fire-induced ET/P modification, results from only our finest-scale MLR models should be used. Further work may help to refine relationships within more homogeneous sub-regions, and non-linear relationships should be considered. Conversely, high burn severity is consistently correlated with greater post-fire ET/P reduction. Because previous studies establish statistical relationships between burn severity and landscape attributes, we posit that an unburned area's post-fire ET/P response may be predictable if a burn severity estimate can be generated first. We also demonstrate that, although the biggest percent ET/P reductions often occur in shrub/scrub landscapes, the biggest magnitude ET_a changes occur in evergreen forests. ET/P recovery rates vary by both location and pre-fire vegetation type, and we identify

relationships between geologically-driven AWC, lithology, and post-fire ET/P response. Land management decisions should account for these nuances by considering which can be managed (e.g., forest composition and structure) and which cannot (e.g., lithology). Because fire activity is increasing in the western CONUS (Parks and Abatzoglou, 2020; Pyne, 2011; Robichaud et al., 2014; van Wagtendonk et al., 2018), our findings highlight the importance of representing the inter-annual processes that control post-fire ET/P change in process-based and statistical hydrological models. Accounting for fire-induced ET/P shifts may be less critical in the eastern CONUS where post-fire ET/P shifts are typically within background levels of the data's natural, interannual variability.

CRediT authorship contribution statement

Natalie M. Collar: Conceptualization, Methodology, Data curation, Formal analysis, Visualization, Writing – original draft, Writing – review & editing. **Samuel Saxe:** Conceptualization, Methodology, Data curation, Writing – review & editing. **Ashley J. Rust:** Conceptualization, Methodology, Writing – review & editing. **Terri S. Hogue:** Conceptualization, Methodology, Writing – review & editing, Supervision, Funding acquisition.

Declaration of Competing Interest

The authors declare that they have no known competing financial interests or personal relationships that could have appeared to influence the work reported in this paper.

Acknowledgements

This work was performed under a Hydrologic Sciences and Engineering fellowship from the Colorado School of Mines and the USGS's Water Availability and Use Science Program. Additional support was provided by a Babbitt Dissertation Fellowship from the Lincoln Institute of Land Policy. All data were obtained from public domains and are freely available. Data generated during the course of this study can be found online at https://doi.org/10.5066/P9LPYOIU (Collar et al., 2021). Any use of trade, firm, or product names is for descriptive purposes only and does not imply endorsement by the US government. The authors thank the anonymous reviewers whose comments and critiques were invaluable.

Appendix A. Supplementary data

Supplementary data to this article can be found online at https://doi.org/10.1016/j.jhydrol.2021.127162.

References

Agee, J.K., 1994. Fire and weather disturbances in terrestrial ecosystems of the eastern Cascades (General Technical Report No. PNW-GTR-320). U.S. Department of Agriculture, Forest Service, Rocky Mountain Research Station, Pacific Northwest Research Station.

Alexander, J.D., Seavy, N.E., Ralph, C.J., Hogoboom, B., 2006. Vegetation and topographical correlates of fire severity from two fires in the Klamath-Siskiyou region of Oregon and California. Int. J. Wildland Fire 15, 237–245. https://doi.org/10.1071/WF05053.

Allen, R.G., Tasumi, M., Trezza, R., 2007. Satellite-based energy balance for mapping evapotranspiration with internalized calibration (METRIC) model. J. Irrig. Drain. Eng. 133 (4), 380–394. https://doi.org/10.1061/(ASCE)0733-9437(2007)133:4(380).

Atchley, A.L., Kinoshita, A.M., Lopez, S.R., Trader, L., Middleton, R., 2018. Simulating surface and subsurface water balance changes due to burn severity. Vadose Zone J. 17 (1), 180099. https://doi.org/10.2136/vzj2018.05.0099.

Bart, R.R., Safeeq, M., Wagenbrenner, J.W., Hunsaker, C.T., 2021. Do fuel treatments decrease forest mortality or increase streamflow? A case study from the Sierra Nevada (USA). Ecohydrology 14 (1). https://doi.org/10.1002/eco.v14.110.1002/eco.2254.

Barton, A.M., Poulos, H.M., 2018. Pine vs. oaks revisited: Conversion of Madrean pine-oak forest to oak shrubland after high-severity wildfire in the Sky Islands of Arizona. For. Ecol. Manage. 414, 28–40. https://doi.org/10.1016/j.foreco.2018.02.011.

Bastiaanssen, W.G.M., Menenti, M., Feddes, R.A., Holtslag, A.A.M., 1998. A remote sensing surface energy balance algorithm for land (SEBAL). 1. Formulation. J. Hydrol. 212–213, 198–212. https://doi.org/10.1016/S0022-1694(98)00253-4.

Battaglia, O.R., Paola, B.D., Fazio, C., 2016. A new approach to investigate students' behavior by using cluster analysis as an unsupervised methodology in the field of education. Appl. Mathematics 07 (15), 1649–1673. https://doi.org/10.4236/am.2016.715142.

Beyene, M.T., Leibowitz, S.G., Pennino, M.J., 2021. Parsing weather variability and wildfire effects on the post-fire changes in daily stream flows: a quantile-based statistical approach and its application. Water Res. 57 (10) https://doi.org/10.1029/2020WR028029.

Bigler, C., Kulakowski, D., Veblen, T.T., 2005. Multiple disturbance interactions and drought influence fire severity in Rocky Mountain subalpine forests. Ecology 86 (11), 3018–3029. https://doi.org/10.1890/05-0011.

Bixby, R.J., Cooper, S., Gresswell, R.E., Brown, L.E., 2015. Fire effects on aquatic ecosystems: An assessment of the current state of the science. Freshwater Science.

Blount, K., Ruybal, C.J., Franz, K.J., Hogue, T.S., 2020. Increased water yield and altered water partitioning follow wildfire in a forested catchment in the western United States. Ecohydrology 13 (1). https://doi.org/10.1002/eco.v13.110.1002/eco.2170.

Boisramé, G.F.S., Thompson, S.E., Tague, C. (Naomi), Stephens, S.L., 2019. Restoring a natural fire regime alters the water balance of a Sierra Nevada catchment. Water Resour. Res. 55, 5751–5769. doi: 10.1029/2018WR024098.

Bond-Lamberty, B., Peckham, S.D., Gower, S.T., Ewers, B.E., 2009. Effects of fire on regional evapotranspiration in the central Canadian boreal forest. Glob. Change Biol. 15, 1242–1254. https://doi.org/10.1111/j.1365-2486.2008.01776.x.

Brunkal, H., Santi, P., 2017. Consideration of the Validity of Debris-Flow Bulking Factors. The Geological Society of America 291–298. doi: 10.2113/gseegeosci.23.4.291.

Buffo, J., Fritschen, L.J., Murphy, J.L., 1972. Direct solar radiation on various slopes from 0 to 60 degrees north latitude. US Forest Service Research Paper PNW-142 75.

Calkin, D.E., Cohen, J.D., Finney, M.A., Thompson, M.P., 2014. How risk management can prevent future wildfire disasters in the wildland-urban interface. Proc. Natl. Acad. Sci. U. S. A. 111 (2), 746–751. https://doi.org/10.1073/pnas.1315088111.

Cansler, C.A., McKenzie, D., 2012. How robust are burn severity indices when applied in a new region? Evaluation of alternate field-based and remote-sensing methods. Remote Sensing 4, 456–483. https://doi.org/10.3390/rs4020456.

Chen, M., Senay, G.B., Singh, R.K., Verdin, J.P., 2016. Uncertainty analysis of the Operational Simplified Surface Energy Balance (SSEBop) model at multiple flux tower sites. J. Hydrol. 536, 384–399. https://doi.org/10.1016/j.jhydrol.2016.02.026.

Collar, Natalie M., Saxe, Samuel, Rust, Ashley J., Hogue, Terri S., 2021. Pixel characteristics for burned SSEBop 1-km pixels over the CONUS. US Geol. Surv. Data Release. https://doi.org/10.5066/P9LPYOIU.

Dai, A., 2017. Global Palmer Drought Severity Index. Research Data Archive at the National Center for Atmospheric Research, Computational and Information Systems Library. doi: 10.5065/D6QF8R93.

Davis, J.C., 2002. Statistics and Data Analysis in Geology, 3rd ed. John Wiley & Sons.

DeBano, L.F., Neary, D.G., Ffolliott, P.F., 1998. Fire Effects on Ecosystems. John Wiley & Sons.

Dias Lopes, J., Neiva Rodrigues, L., Acioli Imbuzeiro, H.M., Falco Pruski, F., 2019. Performance of SSEBop model for estimating wheat actual evapotranspiration in the Brazilian Savannah region. Int. J. Remote Sens. 40 (18), 6930–6947. https://doi.org/10.1080/01431161.2019.1597304.

Dillon, G.K., Holden, Z.A., Morgan, P., Crimmins, M.A., Heyerdahl, E.K., Luce, C.H., 2011. Both topography and climate affected forest and woodland burn severity in two regions of the western US, 1984 to 2006. Ecosphere 2 (12), art130. https://doi.org/10.1890/ES11-00271.1.

Dragosics, M., Meinander, O., Jónsdóttír, T., Dürig, T., De Leeuw, G., Pálsson, F., Dagsson-Waldhauserová, P., Thorsteinsson, T., 2016. Insulation effects of Icelandic dust and volcanic ash on snow and ice. Arab. J. Geosci. 9, 126. https://doi.org/10.1007/s12517-015-2224-6.

Eidenshink, J., Schwind, B., Brewer, K., Zhu, Z.-L., Quayle, B., Howard, S., 2007. A project for monitoring trends in burn severity. Fire Ecol. 3, 3–21. https://doi.org/10.4996/fireecology.0301003.

Elliot, W.J., Miller, I.S., Audin, L., 2010. Cumulative watershed effects of fuel management in the Western United States (No. Rocky Mountain Research Station General Technical Report RMRS-GTR-231). USDA.

Farmer, W.H., Kiang, J.E., Feaster, T.D., Eng, K., 2019. Regionalization of surface-water statistics using multiple linear regression (Techniques and Methods 4-A12), Book 4, Hydrologic Analysis and Interpretation. USGS.

Fernando, D.N., Mo, K.C., Fu, R., Pu, B., Bowerman, A., Scanlon, B.R., Solis, R.S., Yin, L., Mace, R.E., Mioduszewski, J.R., Ren, T., Zhang, K., 2016. What caused the spring intensification and winter demise of the 2011 drought over Texas? Clim. Dyn. 47 (9-10), 3077–3090. https://doi.org/10.1007/s00382-016-3014-x.

Fletcher, T.D., 2012. Package "QuantPsyc.".

Fowler, K., Coxon, G., Freer, J., Peel, M., Wagener, T., Western, A., Woods, R., Zhang, L., 2018. Simulating runoff under changing climatic conditions: a framework for model improvement. Water Resour. Res. 54 (12), 9812–9832. https://doi.org/10.1029/2018WR023989.

Frazier, R., Coops, N., Wulder, M., Hermosilla, T., White, J., 2018. Analyzing spatial and temporal variability in short-term rates of post-fire vegetation return from Landsat time series. Remote Sens. Environ. https://doi.org/10.1016/j.rse/2017.11.007 32-45. https://doi.org/10.1016/j.rse.2017.11.007.

Goeking, S.A., Tarboton, D.G., 2020. Forests and water yield: a synthesis of disturbance effects on streamflow and snowpack in western coniferous forests. J. Forest. 118, 172–192. https://doi.org/10.1093/jofore/fvz069.

Goulden, Michael L., Bales, Roger C., 2014. Mountain runoff vulnerability to increased evapotranspiration with vegetation expansion. Proc. Natl. Acad. Sci. U.S.A. 111 (39), 14071–14075. https://doi.org/10.1073/pnas.1319316111.
Grau Andres, R., 2017. Drought and Fuel Structure Controls on Fire Severity: Effects on Post-fire Vegetation and Soil Carbon Dynamics (Ph.D.). University of Glasgow.
Hallema, Dennis W., Sun, Ge, Bladon, Kevin D., Norman, Steven P., Caldwell, Peter V., Liu, Yongqiang, McNulty, Steven G., 2017. Regional patterns of postwildfire streamflow response in the Western United States: The importance of scale-specific connectivity. Hydrol. Process. 31 (14), 2582–2598. https://doi.org/10.1002/hyp.v31.1410.1002/hyp.11208.
Hallema, D.W., Sun, G., Caldwell, P.V., Norman, S.P., Cohen, E.C., Liu, Y., Bladon, K.D., McNulty, S.G., 2018. Burned forests impact water supplies. Nat Commun 9, 1307. https://doi.org/10.1038/s41467-018-03735-6.
Hankins, D., n.d. Restoring indigenous prescribed fires to California oak woodlands (No. General Technical Report PSW-GTR-251).
Hansen, H., 2018. Wildfire: On the front lines with Station 8. Mountaineer Books.
Häusler, Melanie, Nunes, João P., Soares, Paula, Sánchez, Juan M., Silva, João M.N., Warneke, Thorsten, Keizer, Jan Jacob, Pereira, José M.C., 2018. Assessment of the indirect impact of wildfire (severity) on actual evapotranspiration in eucalyptus forest based on the surface energy balance estimated from remote-sensing techniques. Int. J. Remote Sens. 39 (20), 6499–6524. https://doi.org/10.1080/01431161.2018.1460508.
Hawbaker, Todd J., Radeloff, Volker C., Stewart, Susan I., Hammer, Roger B., Keuler, Nicholas S., Clayton, Murray K., 2013. Human and biophysical influences on fire occurrence in the United States. Ecol. Appl. 23 (3), 565–582.
Hijmans, R.J., van Etten, J., Sumner, M., Cheng, J., Baston, D., Bevan, A., Bivand, R., and others, 2021. Package "raster.".
Horton, J.D., 2017. The State Geologic Map Compilation (SGMC) geodatabase of the conterminous United States. U.S. Geological Survey data release. doi: 10.5066/F7WH2N65.
Jin, Yufang, Randerson, James T., Goetz, Scott J., Beck, Pieter S.A., Loranty, Michael M., Goulden, Michael L., 2012. The influence of burn severity on postfire vegetation recovery and albedo change during early succession in North American boreal forests. J. Geophys. Res. 117 (G1) https://doi.org/10.1029/2011JG001886.
Jones, Gavin M., Gutiérrez, R.J., Block, William M., Carlson, Peter C., Comfort, Emily J., Cushman, Samuel A., Davis, Raymond J., Eyes, Stephanie A., Franklin, Alan B., Ganey, Joseph L., Hedwall, Shaula, Keane, John J., Kelsey, Rodd, Lesmeister, Damon B., North, Malcolm P., Roberts, Susan L., Rockweit, Jeremy T., Sanderlin, Jamie S., Sawyer, Sarah C., Solvesky, Ben, Tempel, Douglas J., Wan, Ho Yi, Westerling, A. LeRoy, White, Gary C., Peery, M. Zachariah, 2020. Spotted owls and forest fire: comment. Ecosphere 11 (12). https://doi.org/10.1002/ecs2.v11.1210.1002/ecs2.3312.
Keeley, Jon E., Keeley, Sterling C., 1984. Postfire recovery of California coastal sage scrub. Am. Midl. Nat. 111 (1), 105. https://doi.org/10.2307/2425548.
Keeley, J.E., 2009. Fire intensity, fire severity and burn severity: a brief review and suggested usage. Int. J. Wildland Fire 18, 116–126. https://doi.org/10.1071/WF07049.
Kettridge, N., Lukenbach, M.C., Hokanson, K.J., Hopkinson, C., Devito, K.J., Petrone, R. M., Mendoza, C.A., Waddington, J.M., 2017. Low evapotranspiration enhances the resilience of peatland carbon stocks to fire: Low peatland evapotranspiration. Geophys. Res. Lett. 44 (18), 9341–9349. https://doi.org/10.1002/2017GL074186.
Key, C.H., Benson, N.C., 2006. Landscape assessment (LA): Sampling and analysis methods (Gen. Tech. Rep. RMRS-GTR-164-CD), Fire Effects Monitoring and Inventory System. Rocky Mountain Research Station, USDA Forest Service, Fort Collins, CO.
Kinoshita, Alicia M, Hogue, Terri S, 2015. Increased dry season water yield in burned watersheds in Southern California. Environ. Res. Lett. 10 (1), 014003. https://doi.org/10.1088/1748-9326/10/1/014003.
Kolden, C.A., Smith, A.M.S., Abatzoglou, J.T., Kolden, C.A., Smith, A.M.S., Abatzoglou, J. T., 2015. Limitations and utilisation of Monitoring Trends in Burn Severity products for assessing wildfire severity in the USA. Int. J. Wildland Fire 24, 1023–1028. https://doi.org/10.1071/WF15082.
Lake, Frank K., Wright, Vita, Morgan, Penelope, McFadzen, Mary, McWethy, Dave, Stevens-Rumann, Camille, 2017. Returning fire to the land: Celebrating traditional knowledge and fire. J. Forest. 115 (5), 343–353. https://doi.org/10.5849/jof.2016-043R2.
Landesmann, Jennifer Brenda, Tiribelli, Florencia, Paritsis, Juan, Veblen, Thomas Thorstein, Kitzberger, Thomas, Collins, Beverly, 2021. Increased fire severity triggers positive feedbacks of greater vegetation flammability and favors plant community-type conversions. J. Vegetation Sci. 32 (1) https://doi.org/10.1111/jvs.v32.110.1111/jvs.12936.
Lau, K-M., Weng, Hengyi, 1995. Climate signal detection using wavelet transform: how to make a time series sing. Bull. Am. Meteorol. Soc. 76 (12), 2391–2402.
Lee, Hyejoo, Malaspina, Dolores, Ahn, Hongshik, Perrin, Mary, Opler, Mark G., Kleinhaus, Karine, Harlap, Susan, Goetz, Raymond, Antonius, Daniel, 2011. Paternal age related schizophrenia (PARS): Latent subgroups detected by k-means clustering analysis. Schizophr. Res. 128 (1-3), 143–149. https://doi.org/10.1016/j.schres.2011.02.006.
Lentile, L.B., Morgan, P., Hudak, A.T., Bobbitt, M.J., Lewis, S.A., Smith, A.M.S., Robichaud, P.R., 2007. Post-fire burn severity and vegetation response following eight large wildfires across the western United States. fire ecol 3, 91–108. https://doi.org/10.4996/fireecology.0301091.
Livneh, B., Deems, J.S., Buma, B., Barsugli, J.J., Schneider, D., Molotch, N.P., Wolter, K., Wessman, C.A., 2015. Catchment response to bark beetle outbreak and dust-on-snow in the Colorado Rocky Mountains. J. Hydrol. 523, 196–210. https://doi.org/10.1016/j.jhydrol.2015.01.039.
Lydersen, J.M., North, M.P., Collins, B.M., 2014. Severity of an uncharacteristically large wildfire, the Rim Fire, in forests with relatively restored frequent fire regimes. For. Ecol. Manage. 328, 326–334. https://doi.org/10.1016/j.foreco.2014.06.005.
Ma, Qin, Bales, Roger C., Rungee, Joseph, Conklin, Martha H., Collins, Brandon M., Goulden, Michael L., 2020. Wildfire controls on evapotranspiration in California's Sierra Nevada. J. Hydrol. 590, 125364. https://doi.org/10.1016/j.jhydrol.2020.125364.
MacQueen, J., 1967. Some methods for classification and analysis of multivariate observations. Fifth Berkeley Symposium: Multivariate Observations 281–297.
Maina, Fadji Zaouna, Siirila-Woodburn, Erica R., 2020. Watersheds dynamics following wildfires: nonlinear feedbacks and implications on hydrologic responses. Hydrol. Process. 34 (1), 33–50. https://doi.org/10.1002/hyp.v34.110.1002/hyp.13568.
Mallakpour, Iman, Villarini, Gabriele, 2016. A simulation study to examine the sensitivity of the Pettitt test to detect abrupt changes in mean. Hydrol. Sci. J. 61 (2), 245–254. https://doi.org/10.1080/02626667.2015.1008482.
Martin, Deborah A., 2016. At the nexus of fire, water and society. Phil. Trans. R. Soc. B 371 (1696), 20150172. https://doi.org/10.1098/rstb.2015.0172.
McCune, Bruce, Keon, Dylan, 2002. Equations for potential annual direct incident radiation and heat load. J. Veg. Sci. 13 (4), 603–606.
McLeod, A.I., 2011. Package "Kendall.".
McShane, R., Driscoll, K., Sando, R., 2017. Scientific Investigations Report: A review of surface energy balance models for estimating actual evapotranspiration with remote sensing at high spatiotemporal resolution over large extents (Scientific Investigations Report), Scientific Investigations Report.
Minnich, Richard A., 2001. An integrated model of two fire regimes. Conserv. Biol. 15 (6), 1549–1553. https://doi.org/10.1046/j.1523-1739.2001.01067.x.
Minnich, Richard A., 1983. Fire mosaics in southern California and northern Baja California. Science 219 (4590), 1287–1294. https://doi.org/10.1126/science.219.4590.1287.
Moritz, M., Batllori, E., Bradstock, R.A., Gill, A.M., Handmer, J., Hessburg, P.F., Leonard, J., McCaffrey, S., Odion, D.C., Schoennagel, T., Syphard, A.D., 2014. Learning to coexist with wildfire. Nature 515. doi: 10.1038/nature13946.
Müller, Marc F., Levy, Morgan C., 2019. Complementary vantage points: Integrating hydrology and economics for sociohydrologic knowledge generation. Water Resour. Res. 55 (4), 2549–2571. https://doi.org/10.1029/2019WR024786.
National Operational Hydrologic Remote Sensing Center, 2004. Snow Data Assimilation System (SNODAS) Data Products at NSIDC, Version 1. Boulder, Colorado USA. National Snow and Ice Data Center. https://doi.org/10.7265/N5TB14TC.
Nolan, R.H., Lane, P.N.J., Benyon, R.G., Bradstock, R.A., Mitchell, P.J., 2015. Trends in evapotranspiration and streamflow following wildfire in resprouting eucalypt forests. J. Hydrol. 524, 614–624. https://doi.org/10.1016/j.jhydrol.2015.02.045.
Nolan, Rachael H., Lane, Patrick N.J., Benyon, Richard G., Bradstock, Ross A., Mitchell, Patrick J., 2014. Changes in evapotranspiration following wildfire in resprouting eucalypt forests. n/a-n/a Ecohydrol.. https://doi.org/10.1002/eco.1463.
Omernik, James M., Griffith, Glenn E., 2014. Ecoregions of the conterminous United States: evolution of a hierarchical spatial framework. Environ. Manage. 54 (6), 1249–1266. https://doi.org/10.1007/s00267-014-0364-1.
Oregon State University, Northwest Alliance for Computational Science and Engineering, 2019. Description of PRISM spatial climate datasets for the conterminous United States.
Parks, S.A., Abatzoglou, J.T., 2020. Warmer and drier fire seasons contribute to increases in area burned at high severity in sestern US forests from 1985 to 2017. Geophys. Res. Lett. 47 https://doi.org/10.1029/2020GL089858.
Pereira, Paulo, Cerdà, Artemi, Lopez, Antonio Jordán, Zavala, Lorena M., Mataix-Solera, Jorge, Arcenegui, Victoria, Misiune, Ieva, Keesstra, Saskia, Novara, Agata, 2016. Short-term vegetation recovery after a grassland fire in Lithuania: The effects of fire severity, slope position and aspect. Land Degrad. Dev. 27 (5), 1523–1534. https://doi.org/10.1002/ldr.v27.510.1002/ldr.2498.
Pewsey, A., 2014. Circular Statistics in R. Oxford University Press.
Pohlert, T., 2020. Package "Trend.".
Poon, P.K., Kinoshita, A.M., 2018. Spatial and temporal evapotranspiration trends after wildfire in semi-arid landscapes. J. Hydrol. 559, 71–83. https://doi.org/10.1016/j.jhydrol.2018.02.023.
Pyne, S.J., 2016. California: A Fire Survey. University of Arizona Press.
Pyne, S.J., 2012. Fire: Nature and Culture. Reaktion Books, London.
Pyne, S.J., 2011. Fire: A Brief History. University of Washington Press.
Reitz, M., Sanford, W.E., Senay, G.B., Cazenas, J., 2017. Annual estimates of recharge, quick-flow runoff, and evapotranspiration for the contiguous U.S. using empirical regression equations. JAWRA J. Am. Water Resour. Assoc. 53 (4), 961–983. https://doi.org/10.1111/jawr.2017.53.issue-410.1111/1752-1688.12546.
Robichaud, P.R., Rhee, H., Lewis, S.A., 2014. A synthesis of post-fire Burned Area Reports from 1972 to 2009 for western US Forest Service lands: Trends in wildfire characteristics and post-fire stabilisation treatments and expenditures. Int. J. Wildland Fire 23, 929–944. https://doi.org/10.1071/WF13192.
Roche, James W., Goulden, Michael L., Bales, Roger C., 2018. Estimating evapotranspiration change due to forest treatment and fire at the basin scale in the Sierra Nevada, California: Forest disturbance and evapotranspiration change. Ecohydrology 11 (7), e1978. https://doi.org/10.1002/eco.v11.710.1002/eco.1978.
Roche, James W., Ma, Qin, Rungee, Joseph, Bales, Roger C., 2020. Evapotranspiration mapping for forest management in California's Sierra Nevada. Front. For. Glob. Change 3. https://doi.org/10.3389/ffgc.2020.00069.
Rodman, K.C., Veblen, T.T., Battaglia, M.A., Chambers, E., Fornwalt, P.J., Holden, Z.A., Kolb, T.E., Ouzts, J.R., Rother, M.T., 2020. A changing climate is snuffing out post-fire recovery in montane forests. Glob. Ecol. Biogeogr. 00, 1–13. https://doi.org/10.1111/geb/13174.

Rother, Monica T., Veblen, Thomas T., 2016. Limited conifer regeneration following wildfires in dry ponderosa pine forests of the Colorado Front Range. Ecosphere 7 (12). https://doi.org/10.1002/ecs2.2016.7.issue-1210.1002/ecs2.1594.

Rouder, Jeffrey N., Engelhardt, Christopher R., McCabe, Simon, Morey, Richard D., 2016. Model comparison in ANOVA. Psychon. Bull. Rev. 23 (6), 1779–1786. https://doi.org/10.3758/s13423-016-1026-5.

Rousseeuw, P., 1987. Silhouettes, a graphic aid to the interpretation and validation of cluster analysis. J. Comput. Appl. Math. 20, 53–65.

Sanford, W.E., Selnick, D.L., 2013. Estimation of evapotranspiration across the conterminous United States using a regression with climate and land-cover data. JAWRA J. Am. Water Resour. Assoc. 49, 217–230. https://doi.org/10.1111/jawr.12010.

Savoca, M., Senay, G.B., Maupin, M., Kenny, J., Perry, C., 2013. Scientific Investigations Report (Scientific Investigations Report), Scientific Investigations Report.

Saxe, S., Hogue, T.S., Hay, L., 2018. Characterization and evaluation of controls on post-fire streamflow response across western US watersheds. Hydrol. Earth Syst. Sci. 22, 1221–1237. https://doi.org/10.5194/hess-22-1221-2018.

Sellers, W.D., 1965. Physical Climatology. University of Chicago Press.

Senay, G., Budde, M., Verdin, J., Melesse, A., 2007. A coupled remote sensing and simplified surface energy balance approach to estimate actual evapotranspiration from irrigated fields. Sensors 7, 979–1000. https://doi.org/10.3390/s7060979.

Senay, G.B., 2018. Satellite psychrometric formulation of the Operational Simplified Surface Energy Balance (SSEBop) model for quantifying and mapping evapotranspiration. Appl. Eng. Agric. 34 https://doi.org/10.13031/aea.12614.

Senay, Gabriel B., Bohms, Stefanie, Singh, Ramesh K., Gowda, Prasanna H., Velpuri, Naga M., Alemu, Henok, Verdin, James P., 2013. Operational evapotranspiration mapping using remote sensing and weather datasets: a new parameterization for the SSEB approach. J. Am. Water. Resour. Assoc. 49 (3), 577–591. https://doi.org/10.1111/jawr.2013.49.issue-310.1111/jawr.12057.

Senay, G.B., Budde, M.E., Verdin, J.P., 2011. Enhancing the Simplified Surface Energy Balance (SSEB) approach for estimating landscape ET: validation with the METRIC model. Agric. Water Manag. 98 (4), 606–618. https://doi.org/10.1016/j.agwat.2010.10.014.

Senay, G.B., Friedrichs, M., Singh, R.K., Velpuri, N.M., 2016. Evaluating Landsat 8 evapotranspiration for water use mapping in the Colorado River Basin. Remote Sens. Environ. 185, 171–185. https://doi.org/10.1016/j.rse.2015.12.043.

Senay, G.B., Gowda, P.H., Bohms, S., Howell, T.A., Friedrichs, M., Marek, T.H., Verdin, J. P., 2014. Evaluating the SSEBop approach for evapotranspiration mapping with landsat data using lysimetric observations in the semi-arid Texas High Plains. Hydrol. Earth Syst. Sci. Discuss. 11, 723–756. https://doi.org/10.5194/hessd-11-723-2014.

Senay, G.B., Verdin, J.P., Lietzow, R., Melesse, A.M., 2008. Global daily reference evapotranspiration modeling and evaluation. JAWRA J. Am. Water Resour. Assoc. 44, 969–979. https://doi.org/10.1111/j.1752-1688.2008.00195.x.

Senkondo, W., Munishi, S.E., Tumbo, M., Nobert, J., Lyon, S.W., 2019. Comparing remotely-sensed surface energy balance evapotranspiration estimates in heterogeneous and data-limited gegions: a case study of Tanzania's Kilombero Valley. Remote Sensing 11, 1289. https://doi.org/10.3390/rs11111289.

Sexstone, Graham A., Clow, David W., Fassnacht, Steven R., Liston, Glen E., Hiemstra, Christopher A., Knowles, John F., Penn, Colin A., 2018. Snow sublimation in mountain environments and its sensitivity to forest disturbance and climate warming. Water Resour. Res. 54 (2), 1191–1211. https://doi.org/10.1002/wrcr.v54.210.1002/2017WR021172.

Shakesby, R., Doerr, S., 2006. Wildfire as a hydrological and geomorphological agent. Earth Sci. Rev. 74 (3-4), 269–307. https://doi.org/10.1016/j.earscirev.2005.10.006.

Sharma, D.N., Tare, V., 2018. Evapotranspiration estimation using SSEBop method with Sentinel-2 and Landsat-8 dataset. Int. Arch. Photogramm. Remote Sens. Spatial Inf. Sci. XLII–5, 563–566. doi: 10.5194/isprs-archives-XLII-5-563-2018.

Silins, Uldis, Stone, Micheal, Emelko, Monica B., Bladon, Kevin D., 2009. Sediment production following severe wildfire and post-fire salvage logging in the Rocky Mountain headwaters of the Oldman River Basin, Alberta. Catena 79 (3), 189–197. https://doi.org/10.1016/j.catena.2009.04.001.

Singh, R., Senay, G., 2015. Comparison of four different energy balance models for estimating evapotranspiration in the midwestern United States. Water 8, 9. https://doi.org/10.3390/w8010009.

Smith, Hugh G., Sheridan, Gary J., Lane, Patrick N.J., Nyman, Petter, Haydon, Shane, 2011. Wildfire effects on water quality in forest catchments: A review with implications for water supply. J. Hydrol. 396 (1-2), 170–192. https://doi.org/10.1016/j.jhydrol.2010.10.043.

Stevens-Rumann, Camille S., Prichard, Susan J., Strand, Eva K., Morgan, Penelope, 2016. Prior wildfires influence burn severity of subsequent large fires. Can. J. For. Res. 46 (11), 1375–1385. https://doi.org/10.1139/cjfr-2016-0185.

Tobin, K., Bennett, M., 2019. Improving alpine summertime streamflow simulations by the incorporation of evapotranspiration data. Water 11, 112. https://doi.org/10.3390/w11010112.

USDA Forest Service, 2003. Influence of forest structure on wildfire behavior and the severity of its effects: An overview.

USDA Forest Service, USDI, n.d. Landfire: Landscape fire and resource management planning tools [WWW Document]. URL https://www.landfire.gov/about.php (accessed 8.17.20).

USDA NRCS, n.d. SSURGO/STATSGO2 structural metadata and documentation, NRCS Soils.

USGS EROS Customer Services, n.d. Landsat provisional actual evapotranspiration [WWW Document]. URL https://www.usgs.gov/core-science-systems/nli/landsat/landsat-provisional-actual-evapotranspiration (accessed 1.22.21).

van Wagtendonk, J., Sugihara, N., Stephens, S.L., Thode, A.E., Shaffer, K.E., Fites-Kaufman, A., Agee, J.K., 2018. Fire in California's ecosystems.

Vanderhoof, M.K., Williams, C.A., 2015. Persistence of MODIS evapotranspiration impacts from mountain pine beetle outbreaks in lodgepole pine forests, south-central Rocky Mountains. Agric. For. Meteorol. 200, 78–91. https://doi.org/10.1016/j.agrformet.2014.09.015.

Velpuri, N.M., Senay, G.B., Singh, R.K., Bohms, S., Verdin, J.P., 2013. A comprehensive evaluation of two MODIS evapotranspiration products over the conterminous United States: Using point and gridded FLUXNET and water balance ET. Remote Sens. Environ. 139, 35–49. https://doi.org/10.1016/j.rse.2013.07.013.

Westerling, Anthony LeRoy, 2016. Increasing western US forest wildfire activity: sensitivity to changes in the timing of spring. Phil. Trans. R. Soc. B 371 (1696), 20150178. https://doi.org/10.1098/rstb.2015.0178.

Whitman, Ellen, Parisien, Marc-André, Thompson, Dan K., Hall, Ronald J., Skakun, Robert S., Flannigan, Mike D., 2018. Variability and drivers of burn severity in the northwestern Canadian boreal forest. Ecosphere 9 (2), e02128. https://doi.org/10.1002/ecs2.2128.

Wickham, J., Homer, C., Vogelmann, J., McKerrow, A., Mueller, R., Herold, N., Coulston, J., 2014. The Multi-Resolution Land Characteristics (MRLC) consortium — 20 years of development and integration of USA National Land Cover Data. Remote Sensing 6, 7424–7441. https://doi.org/10.3390/rs6087424.

Zhang, L., Dawes, W.R., Walker, G.R., 2001. Response of mean annual evapotranspiration to vegetation changes at catchment scale. Water Resour. Res. 37 (3), 701–708.

Zhou, Changrang, van Nooijen, Ronald, Kolechkina, Alla, Hrachowitz, Markus, 2019. Comparative analysis of nonparametric change-point detectors commonly used in hydrology. Hydrol. Sci. J. 64 (14), 1690–1710. https://doi.org/10.1080/02626667.2019.1669792.